TECHNISCHE UNIVERSITÄT WIEN

VIENNA UNIVERSITY OF TECHNOLOGY

Masterarbeit

Photorealistic Rendering Of Measured BRDF Data

Ausgeführt am Institut für
Computergrafik und Algorithmen
der Technischen Universität Wien

unter der Anleitung von
Univ.Prof. Dipl.-Ing. Dr.techn. Werner Purgathofer
und Mitwirkung von
Dipl.-Ing. Andrea Weidlich

durch

Murat Sari bakk. techn.

Salzlände 15/10/47
A-8700 Leoben

Wien, am 1. Mai 2008

Contents

Kurzfassung

Fotorealistisches Rendering von gemessenen Oberflächendaten hat ein grosses Anwendungsfeld, in erster Linie werden die Daten verwendet um Referenzbilder für Analytische Oberflächen-Modelle zu erzeugen. Bevor die Daten für die Erzeugung von Referenzbilderen verwendet werden können müssen diese zuerst gemessen, gefittet und interpoliert werden. In dieser Diplomarbeit werden zwei BRDF (Bidirectional Reflectance Distribution Function) Datenbanken für gemessene Oberflächendaten, die von zwei verschiedenen Universitäten gemessen wurden, für die Simulation verwendet. Eine Datenbank enthält die Oberflächendaten in Form von Spektral Messungen und die andere Datenbank enthält die Messungen im RGB Format. Weiteres werden verschiedene Oberflächen-Modelle und grundlegende Monte Carlo Sampling Methoden betrachtet.

Die grundlegende Aufgabe der Diplomarbeit war es die gemessenen Oberflächendaten in das Advanced Rendering Toolkit (ART) einzubauen um diese für das Rendering zu verwenden. Das Advanced Rendering Toolkit wird seit 1996 auf der TU-Wien vom Institut für Computergraphik und Algorithmen entwickelt. Zusätzlich werden zu den gerenderten Bildern auch Polar Diagramme erzeugt, welche die Reflektionseigenschaften der Materialien zeigen.

Abstract

Photo realistic rendering of measured data is a widely used method to generate reference images for analytical models. But before we can render measured data it has to be acquired and then fitted and interpolated. In this thesis we review two BRDF (Bidirectional Reflectance Distribution Function) databases from different Universities. One database consists of Spectral data where the other only measured the materials in RGB color space. Furthermore we introduce the reader in the basic BRDF models and in the basics of Monte Carlo sampling methods.
We integrate the rendering of measured BRDF data in the Advanced Rendering Toolkit (ART), which is developed since 1996 from the Institute of Computer Graphics and Algorithms of the Vienna University of Technology. Also we evaluate the generated images, with polar plots, to show their reflectance property. Also we show our trilinear interpolation approach, which was used for the data from the Cornell University. To present our work we also rendered several images with the ART pathtracer.

Chapter 1

Introduction

1.1 Light Basics

1.1.1 Historic Background

First some facts about the historical development of light theory. Christiaan Huygens [Huy78] proposed a wave theory of light, he demonstrated how waves interfere to form a wavefront and propagate in a straight line. With his theory he was able to derive the laws of reflection and refraction, but with his wave theory he had difficulties to describe the behavior of other materials. Isaac Newton [New04] published his light theory in 1704, according his theory light is composed of tiny particles, with his theory he was able to describe reflection and also refraction through a lens.
The particle theory of Newton [New04] dominated until Thomas Young [You02] showed, in his experiments, that light behaves like an electromagnetic wave. In 1803 Thomas Young [You02] studied interference and diffraction of light. His experiment consist of a light source and a plane, with two narrow slits inserted, which is between the light source and the detector plane. Waves from one slit are superimposed with waves from the other slit, so they produced a interference pattern on the detector plane with alternate bright and dark lines. In 1905 Albert Einstein [Ein5a] created the quantum theory of light, a quantum is a tiny packet of energy with no mass. Einstein demonstrated with the photoelectric effect experiment that the wave theory alone was not enough. In the end of 1905 Einstein [Ein5a] also showed that light can behave as a continues wave. So this behavior is called the duality of light, waves and particles co-exist at the quanta level.

1.1.2 Nature Of Light

Light in the particle model consists of tiny packets of energy. These particle can be reflected or refracted by matter. Every time a particle is reflected or refracted, an amount of the energy is transferred into heat. The particle packets travel until all the energy is transferred in another form of energy, the energy conservation implies that no energy disappear but the energy will be transformed in a other form.
Light has all the basic properties of an electromagnetic wave like an amplitude, wavelength, phase, frequency and speed. Because the speed of light is constant it is possible to match a single frequency to exact one wavelength. The phase in vacuum, can be different between two waves. If two waves overlap, they interfere with each other, as shown in Figure 1.1 The interference can be constructive or destructive. Constructive interference occurs when two interfering waves have a displacement (amplitude) in the same direction, then the amplitude of the resulting wave is the sum of the amplitudes of the two waves at a discrete point. Destructive interference occurs when two waves have a displacement in the opposite direction, so that the resulting amplitude is the difference between the amplitudes of the two waves.

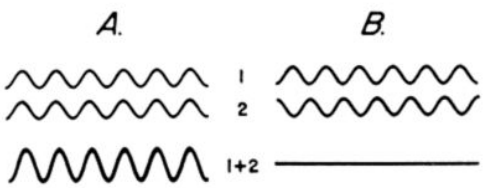

Figure 1.1: Interference between waves: A shows the constructive interference; B shows the destructive interference (image taken from [Wil])

1.1.3 Light And Color

Electromagnetic spectrum that is visible for the human eye, has a range from 380 to 750 nm. These wavelength λ are perceived as colors. Due the fact that the spectrum is continues there are no real boundaries between colors, but here is an approximation table:

Color	Wavelength [nm]
violet	380–450
blue	450–495
green	495-570
yellow	570–590
orange	590-620
red	620-750

Table 1.1: Visible Spectrum

For color perception three components needed: a light source, an object and a detector (in our case the eye) [JN86]. The light source emits light energy which hits, for example, a blue ball. This ball absorbs all frequencies of visible light, which comes from the light source, except the frequencies that are perceived from the eye (the detector) as blue color.
The human eye has three types of color receptors, which are known as cone cells, and each of them has a different spectra response curve. The three groups of cone types are defined as:

- L: they responds most to light of long wavelengths, where λ is between 500-700 nm
- M: they responds most to light of medium wavelengths, where λ is between 450-630 nm
- S: they responds most to light of short wavelengths, where λ is between 400-500 nm

Cones are less sensitive to light, but the human eye has rod cells which are more light sensitive (rods are responsible for night vision). Rods and cones are mutually interconnected and perform pre-processing tasks like edge enhancement.
The LMS cones are color sensitive, also known as RGB sensors, and the rods are luminance sensitive, also known as H (hue). The RGBH signal is converted into the L*a*b color space.
We do not go any deeper in color science in the scope of this thesis, of course there is much more to learn about it. There are three main interactions when light hits matter, in Figure 1.2 we illustrate it, they are reflection, absorption and transmittance. The interactions with light depends on the physical composition and characteristics of the material and the physical composition of light. Figure 1.2 shows following items:

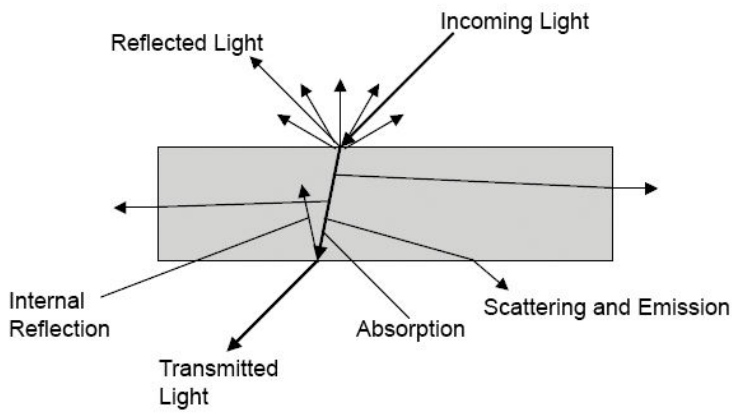

Figure 1.2: General light interaction with a matter; Incoming Light: the light energy which is emitted from a light source; Reflected Light: the amount of light which is reflected; Internal Reflection: the amount of light which is reflected within the matter; Transmitted Light: light which go through the matter; Absorbtion: light which is absorbed in the matter; Scattering and Emission: light which is reflected internal and remitted (image taken from [Wyn00])

1.2 Radiometry

Light is a form of energy and it is measured in Joules. 1 Joule is defined by energy in Watt times unit time.
The ideal light source is a point light source which emits the light energy in all directions uniformly. However most light sources are not ideal emitter and do not equally emit light energy. To measure the energy which is emitted in a certain direction we talk about energy per solid angle or differential solid angle. The solid angle is a surface patch (as shown in Figure 1.3) on the unit sphere and is defined as:

$$dw = (height)(width)$$

$$dw = (d\theta)(sin\theta d\varphi)$$

$$dw = sin\theta d\theta d\varphi$$

(θ, ϕ) is a direction in spherical coordinates (we will describe in the Appendix A what spherical coordinates are) and angular changes $d\theta, d\phi$ describe the solid angle. The unit of the solid angle is $\frac{1}{steradian}$, the aberration of steradian is sr. A unit sphere has 4π steradian energy.

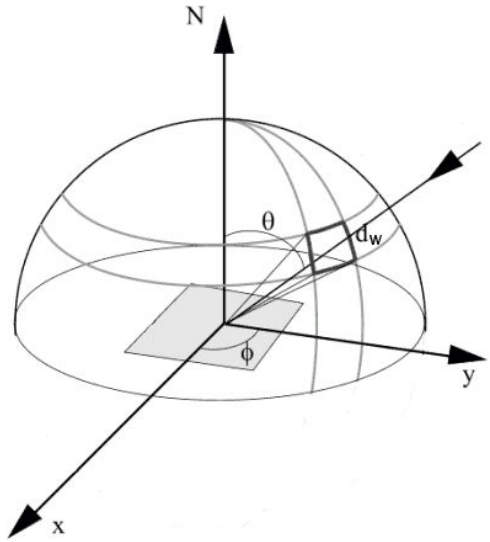

Figure 1.3: Solid angle d_w on the unit sphere (image taken from [Geb03])

1.2.1 Radiance

Radiance is the measure of light energy which is emitted in a certain direction. When we talk about radiance in connection with the wavelength, we mean the whole electromagnetic spectrum and not only the range of the visible light. When we talk about luminance we mean only the visible spectrum, exactly speaking, luminance is defined as photometrically weighted light energy that leaves the surface.

1.2.2 Irradiance

Irradiance is the amount of energy which is received at a surface point. As in the case of radiance we talk also about the whole spectrum; if we only talk about the visible spectrum, we talk about illuminance. The irradiance is defined as energy per area. If we move the light source away from the surface, the energy which arrives at the surface is reduced proportional to the inverse square distance.

1.3 Rendering Equation

A surface is visible to human perception when a light source exists, so what we need is a way to describe the light transport in a scene.
Kajiya [Kaj86] introduced 1986 the rendering equation, which describes the light

transport in a scene with one equation. The definition of the rendering equation is

$$I(x,x') = g(x,x') * [e(x,x') + \int_S p(x,x',x'') * I(x',x'') * dx''] \tag{1}$$

where:

- $I(x,x')$ is the light energy which pass from a point x' to point x.
- $g(x,x')$ is the geometry term which is usually $\frac{1}{r^2}$ where r is the distance between the points and it is zero if one of them is occluded.
- $e(x,x')$ the emission term defines how much light energy is emitted from x' to x.
- $p(x,x',x'')$ how much light energy is scattered from x'' to x through a patch of surface x'; it encodes how light from a given direction is modified upon reflection from a surface.
- $\int_S$ is the integral over $S = \bigcup S_i$, the union of all surfaces.

Equation (1) is a Fredholm Integro-differential of second grade which is impossible to solve analytically, due its recursive nature. The rendering equation can be described as a pair of two points (as above) or for a point and a direction.

$$I(x,\omega) = I_e(x,\omega) + \int_\Omega f_r(x,\omega',\omega) * I(x,\omega')(\omega'.n) * d\omega' \tag{2}$$

where:

- $I(x,\omega)$ is the light energy from point x in direction ω
- $I_e(x,\omega)$ emitted from point x in direction ω
- $f_r(x,\omega',\omega)$ is the BRDF, which defines the proportion of light energy that is reflected at the position x
- $I(x,\omega')$ is the incoming light energy from the position x and direction ω'
- $(\omega'.n')$ is the attenuation of the incoming light energy due to incident angle
- $\int_\Omega$ is the integral over the complete hemisphere

1.4 BRDF

The Bidirectional Reflectance Distribution Function (BRDF) definition depends on the radiance / irradiance ratio. As we already mentioned, radiance tells us how much light energy a point distritbute and irradiance,the counterpart to radiance, tells us how much light energy arrives on a surface patch.
The BRDF is given by:

$$f_r(\omega_i \rightarrow \omega_r) = \frac{I_r(\omega)}{I_i(\omega_r)cos(\theta_i)d\omega_r} \tag{3}$$

- $f_r(\omega_i \rightarrow \omega_r)$ is the BRDF with the unit $\frac{1}{sr}$
- $I_r(\omega)$ is the radiance
- $I_i(\omega_r)cos(\theta_i)d\omega_r$ is the irradiance, the cosine is the projection from the solid angle to the surface patch

Equation 3 shows that the BRDF is not in the range [0,1] because of the cosine term. The vectors ω_r and ω_o are normally parameterized through spherical coordinates. In spherical coordinates a vector is described through two angles, the azimuth angle ϕ and the decline angle θ, both illustrated in Figure 1.4. How to calculate a vector to spherical coordinate and back to cartesian coordinates is described in the appendix A.

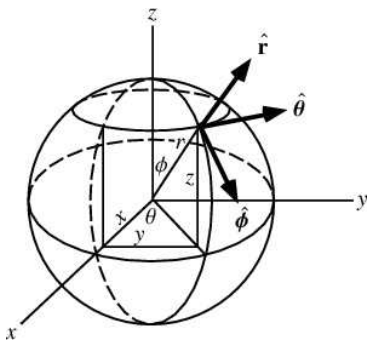

Figure 1.4: Spherical coordinates: θ the azimuthal angle in the x, y plane; ϕ is the polar angle from the z-axis; r is the distance from the origin. (image taken from [Wei])

In the next chapter we present several BRDF models which different material types.

1.4.1 Properties

Each BRDF has two fundamental properties. The first is that they reciprocity has to be valid. That means if we swap the incoming ray and the outgoing ray the resulting reflectance value must be the same.

$$f_r(\omega_i \rightarrow \omega_r) = f_r(\omega_r \rightarrow \omega_i) \tag{4}$$

The second property is that the energy conservation law holds.

$$\int_{\Omega} f_r(\omega_i \rightarrow \omega_r) <= 1 \tag{5}$$

The first property is important for raytracing application. Due the symmetry it does not matter if we shoot rays from the eye or if we shoot rays from the light source, the result must be same. But we also can save storage memory of measured BRDF's, with the first property, because we only need to store the half hemisphere.
The second property guarantees that a surface is not emitting more energy than the incoming light energy. Violating this property would result in a BRDF which would glow. Not every BRDF full fill the last property. Also note that these properties are unique to reflection.

1.4.2 Isotropic And Anisotropic Materials

These two classes of BRDF surfaces define a certain behavior dependant on the viewers position and orientation. So anisotropic material change their reflection behavior when the viewing angle is changed, brushed metal is e.g. an example for an anisotropic material. The exact definition is that reflectance properties change with respect to rotation of the surface around the normal vector.
Anisotropic materials can also change the reflection in a dynamic manner, the human skin is an example for this behavior. But most of the materials are almost rotation invariant, so we can ignore the anisotropic effect for them.
Isotropic materials do not depend on the viewer angle, smooth plastic or paints are e.g. examples for isotropic materials. That means that the BRDF for a isotropic material only needs 3 parameters to describe the reflectance. These parameters are $\Theta_i, \Theta_r, \Phi_{diff}$. The parameter Φ_{diff} do not need any alignment in world space its defined as the difference between Φ_i and Φ_r, the angles are shown in Figure 1.3.

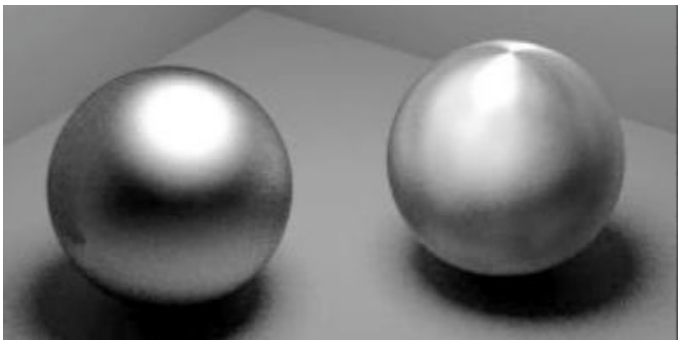

Figure 1.5: Left a isotropic material; Right a anisotropic material (image taken from [Geb03])

1.4.3 Beyond BRDF's

The BRDF is restricted to describe the reflection of a surface, where the bidirectional transmittance distribution function (BTDF), describes the transmission part of the surface. The BTDF is restricted to the other side of the sphere as we can see in Figure 1.6. The bidirectional scattering distribution function (BSDF) is the union of BRDF and BTDF on each side of the sphere, so BSDF is defined over a unit sphere.
We define the symmetry property for a general BSDF:

$$\frac{f_r(\omega_i \rightarrow \omega_r)}{{\eta_r}^2} = \frac{f_r(\omega_r \rightarrow \omega_i)}{{\eta_i}^2} \tag{6}$$

Where η_i, η_r are the refractive indices of the materials. The energy conservation law is also defined for the BSDF.
However the BSDF formalism has several disadvantages. One is that it cannot encode subsurface scattering effects. Thus, a more general formalism is needed, namely the bidirectional surface scattering reflectance function (BSSRDF). The BSSRDF is defined as:

$$S(x_i, y_i, \theta_i, \phi_i, x_r, y_r, \theta_r, \phi_r) \tag{7}$$

The BRDF is actually a special case of the BSSRDF where we assume that light enters and leaves at the same surface point. BSSRDF are quite expensive to solve. When light is reflected many times in a material the details of a single scattering becomes unimportant and the appearance is approximated by diffusing the light away from the enter position.

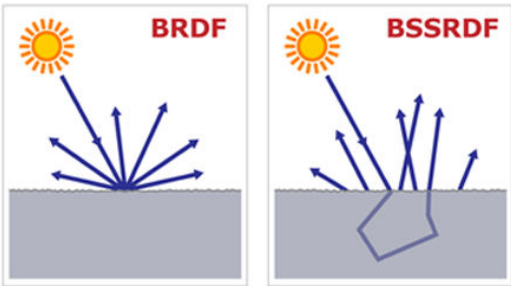

Figure 1.6: Left: BRDF describes the reflection off the surface; Right: BRDF + BTDF describes light rays which are reflected through the microfacet structure of the surface. (image taken from [Wik])

1.5 Purpose and Outline

The main purpose of thesis is to integrate measured BRDF data from the Mitsubishi Electric Research Laboratories (merl) [MPBM03] and data from the Cornell University in ART (Advanced Rendering Toolkit). ART is a photorealistic rendering toolkit which is developed by the Institute of Computer Graphics and Algorithms of the Vienna University of Technology.
The merl database has over 100 isotropic materials which are very dense measured, the color space of the data is RGB. To calculate the solid angle for each ray pair we had to resample the data once for each material. The Cornell database has 11 different isotropic materials, the measurement are present as spectral data in different sampling rates and are also present as RGB data without any gamut mapping, the data contains negative red values. The main purpose of this is to generate reference images to test the analytical surfaces in other words to create ground truth images.
In the next chapter we present different reflectance models then we talk about BRDF acquisition and describe the acquisition process. The chapter about Monte Carlo renderings introduces the reader in the basics of the Monte Carlo methods which are essential for image synthesis. Finally we show our implementation and the rendering results.

Chapter 2

Representing BRDFs

There are different ways to describe materials through a BRDF representation. The first way is the measure and fit approach-we could measure a material with a Gonioreflectometer and use the measured data for the rendering. Measuring a surface is time consuming and could take several hours ([Mat03]). The fact that the BRDF is a four dimensional function makes the measuring process technical challenging, but the measuring approach is necessary for verification purposes, although thats not the only area where measured data are needed.
For example, the NASA has a Reflectometer(SOC-200) which they use to design paints for Stealth aircrafts. These paints absorb and reflect electromagnetic waves in the wrong direction and making the painted object invisible for the radar. Measured BRDF's are also used in the movie "The Matrix 2" for realistic cloth rendering ([Bor03]).
Another representation of BRDF is the approximation through analytical reflectance models. The two types of analytical reflectance models are the physical plausible models and empirical reflectance models (also known as phenomenological reflectance model). Physical plausible reflectance models try to take care of the physical properties of the material, so that each parameter has a physical meaning, and could be theoretically measured. Empirical (or phenomenological) reflectance models describing reflectance with parameters that do not have any physical mean such as the Phong [Pho75] reflectance model. But before we describe some BRDF models, we present some material classification in the next section.

2.1 Material Classification

We already introduced isotropic and anisotropic materials. Now we introduce optical material properties for material classification: ideal diffuse, ideal specular,

directional diffuse and rough specular.

- **Ideal diffuse** reflectors e.g. chalk, clay some paints have - at the microscopic level - a very rough surface. This microscopic variations reflect the incoming light equally in all directions over the hemisphere. The reflection is view direction independent.
- **Ideal specular** reflectors are perfect mirrors, where the microscopic elements are oriented in same direction as the surface. The reflection is view independent and the light rays bounce off the surface in a mirror like fashion.
- **Rough specular** reflectors reflect light not only in the ideal direction - because of microscopic surface variations. Some of the light is reflected slightly offset from the ideal specular angle.
- **Directional diffuse** reflectors are a combination (superposition of BRDF's) of a rough specular reflector and an ideal diffuse reflector. This reflector type is difficult to model analytically.

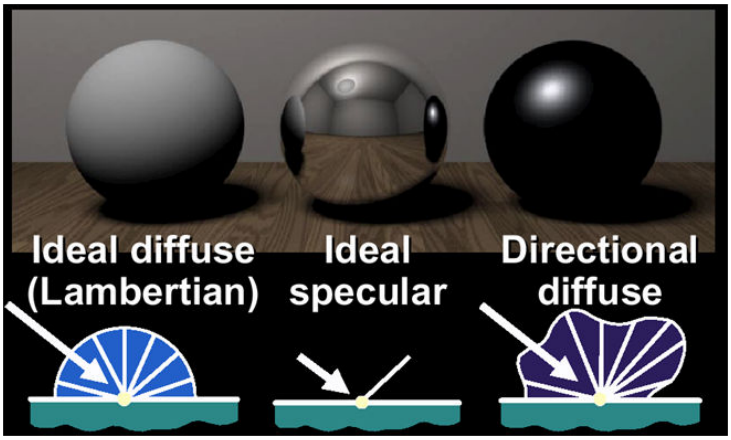

Figure 2.1: Left: A sphere rendered with a ideal diffuse reflector; Middle: A sphere rendered with a ideal specular reflector; Right: A sphere rendered with a directional diffuse. (image taken from [Hua02])

2.2 Empirical Reflectance Models

As we mentioned earlier empirical reflectance models or phenomenological models have no physical meaning but they are approximations of different surface behaviors.

2.2.1 Lambert Reflectance Model

The Lambert reflectance model is a simple model to describe diffuse reflection of a surface. The model it self is defined by Johann Heinrich Lambert [Lam] over 250 years ago. The Lambertian model reflects the indicant light equally in all directions. A Lambertian reflector is independent from the viewing direction, it only depends on the angle Θ which is defined as the cosine between surface normal and indicant light vector.
The Lambertian distribution function is defined as :

$$f_r(\lambda) = \frac{1}{\pi} * k_d(\lambda)$$

The color is wavelength dependent. k_d is defined through $k_d = cos(\Theta_i)$, Lamberts cosine law. The light energy which leaves the Lambertian surface is proportional to the cosine of Θ_i.

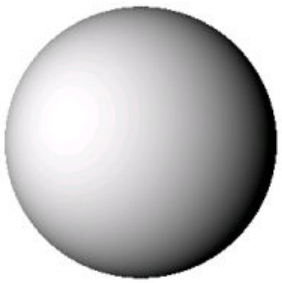

Figure 2.2: A diffuse sphere using the Lambert reflectance model. (image taken from [Geb03])

2.2.2 Phong Reflectance Model

1975 Phong Bui Tong developed the Phong model [Pho75], the original model is not physically plausible. Phong extended the Lambert model with a specular term.
The Phong specular term is defined as:

$$f_r(l,v) = k_s * \frac{(v \cdot r)^{spec_{exp}}}{n \cdot l}$$

Where l is the light vector (vector from the surface point to the light source), v is the view vector (from viewer to the surface point), r reflection vector (in which direction the light is reflected), k_s is the specular coefficient and $spec_{exp}$ is the specular exponent. For this model, Phong made two assumptions, namely all light sources are moved to infinite and that the viewer is also moved to infinite.
Since this equation only describes the specular term, the full equation is the sum (superposition) of the diffuse (Lambert) term and the specular term:

$$f_r(l,v) = \frac{1}{\pi} * k_d + k_s * \frac{(v \cdot r)^{spec_{exp}}}{n \cdot l}$$

There is also a modification of the Phong model by Lewis [Lew93] which make it physical plausible.

2.2.3 Lafortune Reflectance Model

The Lafortune et al. [LFTG97] model is a generalization of the cosine lobe model from Lewis which is based on the Phong model. Lafortune et al. [LFTG97] developed a model which can describe various BRDFs like non-Lambertian diffuse reflection, specularity at grazing angles, off-specular reflection, retro reflection and anisotropic reflection. The main drawback of the original cosine lobe model is that there are several problems with directional-diffuse reflectance.
The definition of the generalization of the classical cosine lobe model is:

$$f_r(L,V) = \frac{k_d}{\pi} + k_s(L^T MV)^n$$

where:

- L is the unit vector to the light source
- V is the unit view vector
- k_d is the diffuse coefficient
- k_s is the specular coefficient
- M is 3 x 3 matrix which must be symmetric; otherwise the Helmholtz reciprocity would not hold
- n is the specular exponent

After singular value decomposition of the matrix M we get $M = Q^T DQ$. Where Q is the transformation of the local coordinate system and D is a diagonal matrix.
Now we can rewrite model as:

$$f_r(L,V) = \frac{k_d}{\pi} + k_s(C_x L_x V_x + C_y L_y V_y + C_z L_z V_z)^n$$

With the parameters C_x, C_y and C_z we can form several BRDF models. For a isotropic reflection the parameter C_x and C_y have to be equal.
To get the original cosine lobe the parameters have to following appearance $-C_x = -C_y = -C_z = \sqrt[n]{C_s}$. To gain an anisotropic reflection the parameters C_x, C_y and C_z must assigned with different values. These parameters are described in detail in [LFTG97].

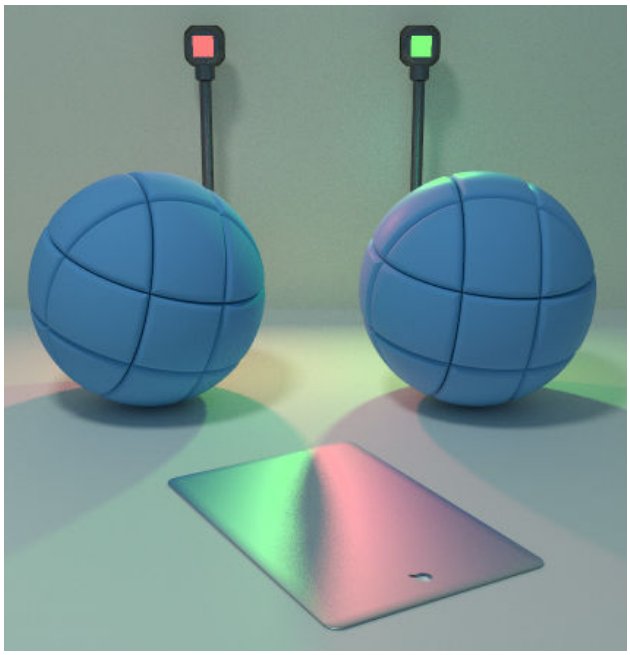

Figure 2.3: Rendered picture of a scene with two spheres and a Q-panel, illuminated by two colored light sources and one larger white light source. The sphere on the left has a Lambertian approximation of the measured paint reflectance; the sphere on the right is rendered with the non-linear approximation. The Q-panel has the non-linear approximation of the measured steel reflectance.(image taken from [LFTG97])

2.2.4 Ward Reflectance Model

In the year 1992 Ward [War92] build an image based gonioreflectometer to measure and acquire data from isotropic and anisotropic surfaces. Ward measured rolled brass, rolled aluminum, lightly brushed aluminum, varnished plywood, enamel finished metal and a painted cardboard box also isotropic surfaces measured like glossy grey paper. The measurements of the Ward imaging gonioreflectometer prototype has two limitations. First the prototype is not able to measure near grazing angles. The second limitation is that the prototype is not able to measure polished surfaces with sharp specular peaks.
To use the raw measurement data for the rendering is impractical due the nature of the data. The data is incomplete to represent to whole hemisphere and to noisy. Therefore Ward tried to develop a model which fits the data for the isotropic and anisotropic measurments with as few parameters as possible.
The aim of the Ward model is first to fulfill physical properties (energy conservation, Helmholtz reciprocity) and second to be mathematical simple like the widely used Phong model. The Gaussian distribution, which is often used in formulations of reflectance ([War92], [CT82], [Coo86]), is used to describe the statistical difference of the surface height. The Gaussian model is used instead of the commonly used geometric attenuation factors and the Fresnel coefficient, the geometric factors usually tend to counteract to the Fresnel coefficient Ward [War92].
The isotropic Gaussian Model:

$$f_{ds,iso}(\theta_i,\phi_i,\theta_r,\phi_r) = \frac{f_d}{\pi} + f_s * \frac{1}{\sqrt{cos(\theta_i)cos(\theta_r)}} * \frac{exp[-tan^2\delta/\alpha^2]}{4\pi\alpha^2}$$

where:

- f_d is the diffuse reflectance
- f_s is the specular reflectance
- δ is the angle between the surface normal vector and the half vector
- α is the standard deviation of the surface slope, α should not greater than 0.2 to no violate the normalization
- $\frac{1}{4\pi\alpha^2}$ is the normalization factor

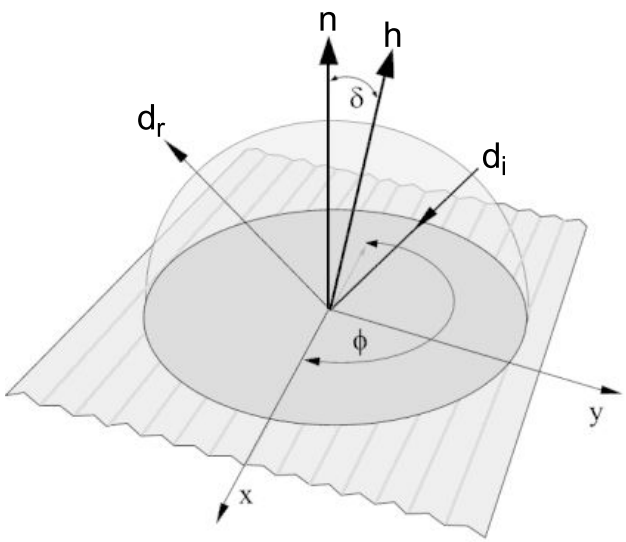

Figure 2.4: Material independent variables and angles which are used in the Ward reflectance model where x and y are the tangents of the surface point, n is the normal vector, h is the half vector between d_r and d_i; *"the indicant light arrives along d_i and is simulated or measured in direction d_r"* Ward [War92]. (image taken from [Geb03] and slightly modified)

The Gaussian reflectance model is extended to support surfaces with two perpendicular slope distributions, α_x and α_y. The anisotropic Gaussian Model is defined as follows:

$$f_{ds}(\theta_i, \phi_i, \theta_r, \phi_r) = \frac{f_d}{\pi} + f_s * \frac{1}{\sqrt{cos(\theta_i)cos(\theta_r)}} * \frac{exp[-tan^2\delta(cos^2\phi/{\alpha_x}^2 + sin^2\phi/{\alpha_y}^2)]}{4\pi{\alpha_x}^2{\alpha_y}^2}$$

where:

- f_d is the diffuse reflectance
- f_s is the specular reflectance
- δ is the angle between the surface normal vector and the half vector
- α_x is the standard deviation of the surface slope in x direction
- α_y is the standard deviation of the surface slope in y direction
- ϕ is the azimuth angle of the half vector projected into the surface plane

A computationally approximation of the above equation is:

$$f_{ds}(\theta_i,\phi_i,\theta_r,\phi_r) = \frac{f_d}{\pi} + f_s * \frac{1}{\sqrt{cos(\theta_i)cos(\theta_r)}} * \frac{1}{4\pi\alpha_x\alpha_y} * exp(-2\frac{(\frac{h\cdot\overrightarrow{x}}{\alpha_x})^2 + (\frac{h\cdot\overrightarrow{y}}{\alpha_y})^2}{1+h\cdot n})$$

where:

- $h\cdot\overrightarrow{x} = \frac{sin\theta_r cos\theta_r + sin\theta_i cos\theta_i}{||\overrightarrow{h}||}$
- $h\cdot\overrightarrow{y} = \frac{sin\theta_r sin\theta_r + sin\theta_i sin\theta_i}{||\overrightarrow{h}||}$
- $h\cdot\overrightarrow{n} = \frac{cos\theta_r + cos\theta_i}{||\overrightarrow{h}||}$
- $||\overrightarrow{h}|| = \sqrt{2 + 2sin\theta_r sin\theta_i(cos\theta_r cos\theta_i + sin\theta_r sin\theta_i) + 2cos\theta_r cos\theta_i}$

The missing variables are described in Figure 2.4. So the total reflectance is the sum of the f_d term (diffuse term) and the f_s term (rough specular term). "α_x *and* α_y *represent the standard deviation of the surface slope in each of the perpendicular directions*" Ward [War92]. All four variables have a physical meaning and could optionally measured.

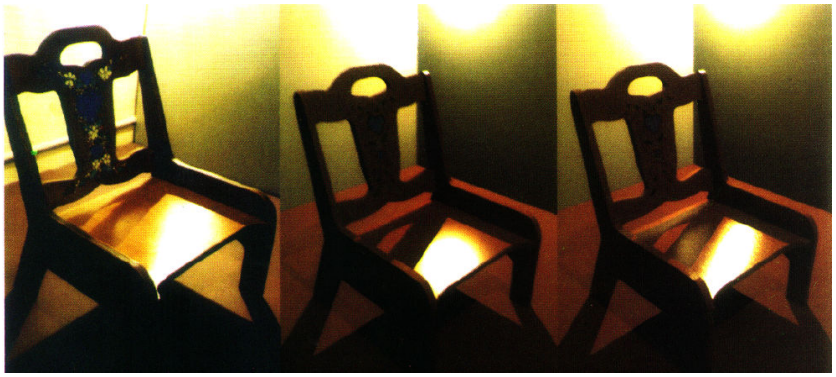

Figure 2.5: Varnished wood comparison. Left: Photograph of a chair; Middle: Use the isotropic Gaussian model for the simulation; Right: The elliptical Gaussian model. (image taken from [War92])

2.3 Physical Plausible Reflectance Models

Physical plausible, physical based or theoretical reflectance models are models where each parameter has a physical meaning or at least they could be measured. In this section we present a few reflectance models but there are a lot more publications e.g. Nayar et al. [SKN91] Blinn [Bli77] Oren, Nayar [ON95].

2.3.1 Cook-Torrance Reflectance Model

The model from Cook and Torrance [CT82], which was published in 1982, is based on the model from Torrance and Sparrow [KET67] and the Blinn [Bli77] reflectance model. The Cook-Torrance model is able to represent different metals like gold but it is also capable to represent plastic with various roughens.
The Torrance-Sparrow model was the first published physically based BRDF model. The calculations of reflectance from roughed surfaces are on the basis of geometrical optics, also the calculations are only valid if the wavelength λ of light is smaller than the least squared mean σ_m of the surface roughness. Also the roughness of the surface is assumed to be isotropic. Furthermore Torrance and Sparrow showed that the assumption that the reflectance of roughed surfaces only occur in form of diffuse reflection only hold if the indicant angle is near to the surface normal vector. But the also showed that the maximum energy occur on a angle which is greater than the specular peak this phenomena is called off specular peak [KET67].
The Cook-Torrance reflectance model is composed from three different components the microfacet distribution, the Fresnel coefficients and the geometric attenuation.
The facets are assumed as mirror-like (perfectly reflective) and isotropic distributed. It is also assumed that the facets are V-shaped, this means that each neighbor has the same slope angle but in the inverse direction. In the Cook-Torrance model it is possible to use different distributions for the microfacet orientations, the Torrance-Sparrow model is restricted to a Gauss distribution, but they make use of the Beckmann distribution function. The geometric term accounts effects of masking and shadowing between microfacets (shown in Figure 2.6), the term determine the amount of the specular reflection.

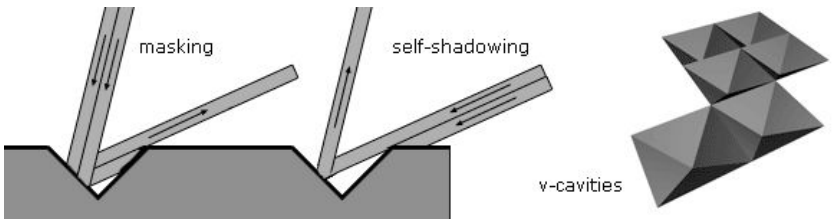

Figure 2.6: Left: shows the masking and self shadowing effects due the microfacet surface structure;Right: show the v-shaped facets. (image taken from [Wyn00])

The geometric term does not depend on any physical property of the surface. The Fresnel term determine the reflection of each microfacet.

The Cook-Torrance model is defined as:

$$f_r(\theta_i, \phi_i, \theta_r, \phi_r) = \frac{k_d}{\pi} + \frac{k_s}{\pi} * \frac{FDG}{cos(\theta_i)cos(\theta_r)}$$

where:

- k_d is the diffuse reflectance coefficient
- k_s is the specular reflectance coefficient
- F is the Fresnel coefficient
- D is the geometric attenuation
- G is the microfacet distribution

With the Cook-Torrance model it was first possible to render rough conductors that have the unique property that their highlights are colored. With simple BRDF models like the Phong model every material looks like plastic because of the white highlight.

Figure 2.7: Several materials simulated with the Cook-Torrance reflectance model (image taken from [CT82])

2.3.2 He-Torrance-Sparrow-Green Reflectance Model

He et. al. [HTSG91] developed as a model which takes the wave nature of light into account to model phenomena like interference and diffraction.

The model consists of three main reflectance components: specular, directional diffuse and uniform diffuse. The model itself is an analytic model which has smooth transitions from the specular to the diffuse reflectance behavior. The specular component accounts mirror like facets, like the Cook-Torrance model, also roughness, shadowing/masking and the Fresnel term is taken into account.
The specular component is the result of the first surface reflection. The directional diffuse is responsible for diffraction and interference effects. The uniform diffuse component estimates that the microfacets are V-shaped, based on geometrical optics. Multiple surface and subsurface reflections result as the uniform diffuse term. The HTSG has several parameters. These are: surface roughness, index of refraction, autocorrelation length and uniform diffuse term. The definition of the reflectance model is the sum of the three components. Due the complex nature of the terms we redirect to the original paper, which is a good starting point for the reader.

Chapter 3

BRDF Acquisition

The BRDF can be directly measured from real surfaces. There are several BRDF data sets available which already measurement. This chapter gives an overview about a device for measuring the BRDF from a surface. Furthermore we review several BRDF measurement databases which are available, free of any charge, for academic purpose.

3.1 Gonioreflectometer

A gonioreflectometer is a device for BRDF acquisition, but there exist several different gonioreflectometer types e.g. Murray etal. [MC75], Foo [Foo97] or Ward [War92].
Murray etal. [MC75] designed a basic gonioreflectometer, which is shown in Figure 3.1. The measuring system consists of a light source, material source and a reflectance detector.

- The **light source** is an MR16 incandescent lamp.
- The **photodetector** is of the silicon photodiode type.
- The **material sample** diameter is only 6.5mm

These three components are positioned with stepper motors, so the system provides the needed four degree of freedom which is required by the - anisotropic - BRDF definition. The stepper motors are controlled by a computer, with ASCII commands, through the RS232 serial port. The system measure *the voltage differential to the illuminance on the face of the photocell* Murray etal. [MC75] for the data acquisition.

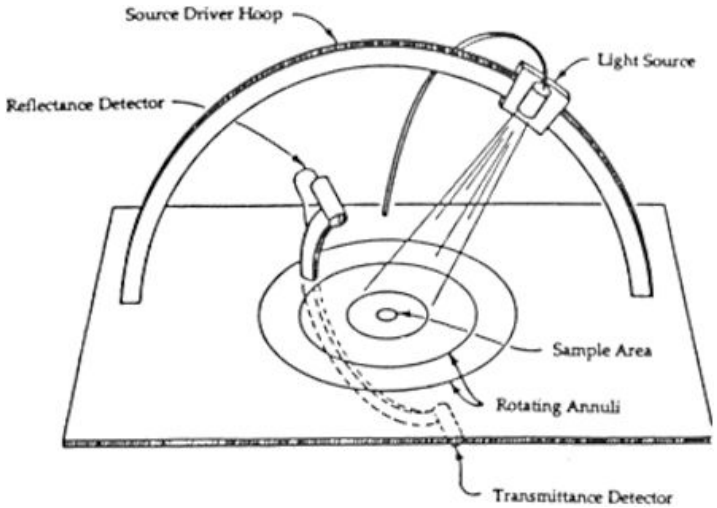

Figure 3.1: Basic gonioreflectometer designed by Murray etal. [MC75] (image taken from [MC75])

In contrast to that Ward [War92] build an imaging gonioreflectometer, namely a silver hemisphere reflectometer. The system consists of a half-silvered hemisphere, a CCD camera with a fish-eye lens, a light source (a three watt quartz-halogen lamp) and a sample holder. The light is reflected from the material to the silver hemisphere which reflect the light onto the CCD array. A computer controlled motor moves the light source during data acquisition and the sample is moved manually.

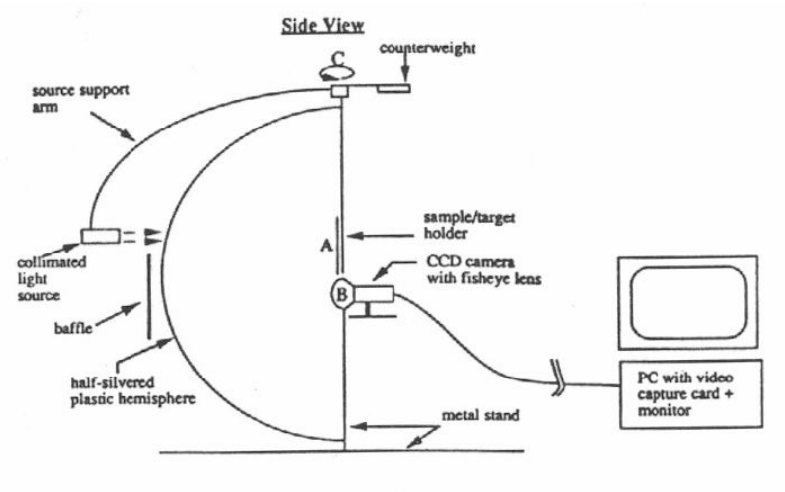

Figure 3.2: Side view of the imaging gonioreflectometer designed by Ward [War92]. (image taken from [War92])

The use of the gonioreflectometer in his ordinary form is slow and time consuming. Ward's imaging gonioreflectometer can obtain BRDF results faster, the hemisphere of reflection is captured in one image, and at lower cost as the traditional approach. The Cornell University [Foo97] extended the imaging approach and built their own device. Matusik [Mat03] also built an imaging gonioreflectometer which is described in the next section.

3.2 BRDF Measurement Databases

In this thesis two BRDF databases are used for the image synthesis, the first one is the database which the Cornell University offers and the second one is offered by the Mitsubishi Electric Research Laboratories (Merl). In the next two sections we take a deeper look how this two databases acquired their BRDF data from the materials. For the sake of completeness the CURet database is also mentioned here, but this one is not used for image synthesis.

3.2.1 CUReT Database

The CUReT database consists of 60 measured materials, the samples are not dense measured approximately 200 reflectance measurements over varying incident and reflected angles (Dana etal. [DvGNK99]). They also offer a BRDF parameter database which fits the parameters for the Oren-Nayar [ON95] and the Koenderink reflectance model ([DvGNK99]).
The samples are not dense enough to use it directly as BRDF lookup table and to generate a reference image (in fact it could be used with interpolation, but then we do not get a meaningful reference image).

3.2.2 Cornell Database

The Cornell University offers also a small BRDF database [LFTG97] which consists of eleven material samples which are all isotropic. The samples are available as spectral, XYZ or as RGB data. Each material sample has over 1000 measurements of varying incident and reflected angles and can be used as BRDF lookup table for direct rendering.
They originally measured 1024 wavelength samples, per sample point, which are down sampled to 65 or 31 wavelengths with a regular sample distance from 5 or 10 nm. They sampled between 400 and 700nm due to the fact that the samplings below 400 and over 700nm are noisy. The raw data, which is available on the Cornell website, has several errors and are not interpolated except the house paint data which is interpolated and cleaned. Unfortunately the measuring process of

the materials are not documented except the house paint [LFTG97] and the acquisition of the skin measuring [MWLT00].

3.2.3 MERL Database

The Mitsubishi Electric Research Laboratories [MPBM03] have the largest isotropic BRDF database and consists of over 100 materials. They build a custom imaging gonioreflectometer for the BRDF acquisition. The device was build with the idea in mind to make dense BRDF measurements which could directly used as a table-based model.
Matusik [Mat03] put the measurement system in an isolated room, the walls in the room were painted with a matte black paint. The gonioreflectometer itself consist of three main components: *"QImaging Retiga 1300 (a 10-bit, and a 1300 x 1030 resolution Firewire camera), a Kaidan MDT-19 (a precise computer-comtrolled turntable), and a Hamamatsu SQ Xenon lamp (a lamp with stable light emission output and a continuous and relatively constant radiation spectrum over the visible light range"*[Mat03]. The light source can move in 0.5 increments. However, to cover the whole hemisphere, the imaging gonioreflectometer needs 330 High Dynamic Range (HDR) images; to capture these images the system needs 4 hours. To get the relative position between light source, camera and material source, a geometric calibration has to be done which is described in detail in [Mat03]. Due to the fact that the camera can only make 10-bit images, they make use of the multi-exposure technique to capture the dynamic range of the scene. So each HDR image is composed from eighteen 10-bit pictures with increasing exposure time.
To compute the BRDF for a pixel one need - beside the radiance of the pixel which is already given by the HDR images - the irradiance for the pixel. To calculate the irradiance, the image pixel is intersected with the sphere to determine the point p on the material source. Then the normal vector of p is calculated. But one also needs the distance to the light source from p and the camera vector. With these variables Matusik was able to calculate the irradiance. Since the BRDF is the ratio between radiance and irradiance, Matusik was able to calculate the BRDF value for a point p on the material source.
The data representation could not done with a regular sampled grid over the hemisphere, even with high tesselated one, because the specular peaks become oval lobes. Rusinkiewicz [Rus04] proposed a new coordinate frame (illustrated in Figure 3.3) which require less storage space for isotropic BRDF's and represent the specular peak efficiently (the new coordinate frame is described in detail in appendix B). With the new coordinate frame [Mat03] was able to use smaller bins near the specular angle, so in fact, the grid is irregular. Matusik subdivide the θ_h and θ_d in 90 bins and ϕ_d in 360 bins, but through the reciprocity property of the

BRDF he cut it to 180 bins down. The resulting data set has 1,458,000 bins per color channel.
The samples are very dense measured and can directly used as tabulated BRDF table or it can be used to create new BRDF's through linear combination of the existent measurements. MERL has also a small BRDF database for anisotropic materials which is - since we concentrated on isotropic BRDF's in the scope of this thesis - not relevant for us. Ngan et. al. [NDM05] have also analyzed the complete isotropic BRDF database and fitted several analytical models to their measurements.

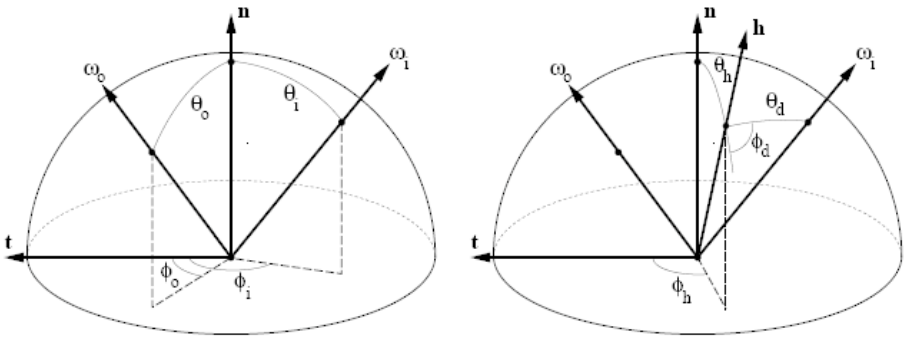

Figure 3.3: Left: ordinary coordinate frame, Right: Rusinkiewicz coordinate frame. (image taken from [Rus04])

In this thesis the Cornell and the isotropic Merl database are used for the image synthesis in ART (Advanced Rendering Toolkit). In the next chapter we take an overview about Monte-Carlo sampling, which we need to sample the BRDF data.

Chapter 4

Monte Carlo Rendering

Scientists introduced the term Monte Carlo in the year 1940 while working on nuclear weapon projects in the Los Alamos National Laboratory. It refers to mathematical techniques that use statistical sampling to solve a problem[1]. Monte Carlo methods have a wide spread application field from the Physical chemistry, Reliability engineering to Computer Graphics.
Monte Carlo raytracing (Jensen [Jen01]) is important for realistic image synthesis from complex scenes. As mentioned in chapter one we have to solve the rendering equation [Kaj86], which describe the light transport in the scene. One way to solve this equation is to use Monte Carlo methods.
In former times finite element methods were the first choice to solve the equation numerically. Finite element methods have several drawbacks, which Monte Carlo methods do not have. With finite element methods the scene geometry must be tessellated, which result in high memory consumption, also not every BRDF can handled with these methods. Also the runtime of Monte Carlo based algorithm are in $O(logN)$, where the fastest finite element method is in $O(NlogN)$. The biggest drawback of Monte Carlo raytracing is the variance seen as noise in the rendered images. There are several methods to decrease the noise which we catch later in this chapter.
This chapter has following structure: first we take an short overview about the basic elements of the probability theory then we discuss Monte Carlo integration and introduce several sampling methods.

[1]There are also Las Vegas methods which use also randomness in their algorithms. The difference between them is that Las Vegas methods use randomness but the give always the correct result in contrast Monte Carlo methods return frequently the wrong result but return the correct result in average.

4.1 Basic Elements Of The Probability Theory

In this section discusses the basic elements of the probability theory. Note that we only discuss a tiny subset of the probability theory. Also note that this is only a review of the basic elements and not a in depth explanation, for an in depth explanation read Kalos and Whitlock [KW86].

4.1.1 Random Variable

A random variable X is defined as an scalar or vector quantity whose values are taken from some domain Ω. The domain Ω can be discrete or continues. A discrete domain is for example all values that can appear when a dice is tossed then X is a random variable defined as $X \in \{1,2,3,4,5,6\}$. Continues random variable X is defined as $X \in \{-\infty,\infty\}$. A distribution of values describes the behavior of the random variable X. Furthermore, the distribution of values can be described by the probability density function (from now on we use the acronym PDF) which we describe in the next section.

4.1.2 Probability Density Function

Usually when a random variable X has a certain PDF p this association is denoted as $X \sim p$. The density function p defines the relative likelihood of a random variable X which takes a certain value.
The PDF must fulfil two properties:

- $p(X) \geq 0$ the probability is always positive (including zero)
- $\int_\Omega p(X)dx$ must integrate to over the domain Ω

4.1.3 Cumulative Distribution Function

The cumulative distribution function (CDF) describes the probability distribution of random variable X. The CDF of X is defined as: $F(X) = \int_\Omega^x p(X)dx$
The CDF must fulfil two properties:

- $\lim_{x \to -\infty} F(X) = 0$
- $\lim_{x \to +\infty} F(X) = 1$

4.1.4 Expected Value

The average or mean of a function f of random variable X with the PDF p is defined as:

$$E(f(X)) = \int f(X)p(X)dX$$

The excepted value has two properties: the excepted value of two random variables X,Y is the same as the sum of the excepted value from X and the excepted value from Y; the previous property can be extend to the usage of functions, because functions of random variables are them self random variables.
We can also estimate the integral by a sum, the method called *theorems of large numbers*, but the variables have to be independent identically distributed and must share the same PDF p. Then the estimate is defined as:

$$E(X) \approx \frac{1}{N}\sum_{i=1}^{N} X_i$$

where N is the number of variables, with the increase of N the variance decreases.

4.1.5 Variance And Standard Deviation

The variance V of random variable is defined as:

$$V(X) = E[(X - E[X])^2]$$

where E is the excepted value of the random variable X. The term above can be simplified as follows:

$$V(X) = E(X^2) - [E(X)]^2$$

The standard deviation is defined as:

$$\sigma(X) = \sqrt{V(X)}$$

where $\sigma(X)$ gives the excepted absolute deviation from the excepted value $E(X)$. The standard deviation is also known as standard error of a random variable X.

4.2 Monte Carlo Integration

The rendering equation is a complicated -Fredholm equation of second grade- integral which is impossible to solve analytically.
Monte Carlo integration break the integration problem down into excepted value problem. As we already mentioned in section 4.1.4, it is possible to estimate a integral with the *theorems of large numbers*. The Monte Carlo algorithm generates

independent random sample points $x_1, x_2, ..., x_i$ with a probability density function p and solve the integral with *theorems of large numbers*. So we only need to be able to evaluate the integrand for specific sample points.
The accuracy of the Monte Carlo integration depends on the number of the sample points and how the get chosen. To halve the estimation error of the Monte Carlo method the sample point count has to be quadrupled. A big advantage of Monte Carlo methods is that the convergence rate does not depend on the dimensionality of the integrand. As we mentioned earlier, the estimation error in Monte Carlo rendering manifests itself as noise in the rendered images. When we sample the integral with ordinary random points we have big holes between the sample points, but to use sample points which are generated on a regular grid is counterproductive because then we get a dependency between the integrand dimension and the efficiency of the estimation [Las99]. To decrease the noise (error) in the images we can generate quasi-random sample points instead of random points. Quasi Monte Carlo use quasi-random numbers (Halton low-discrepancy sequence) which are more evenly distributed as ordinary random generators.

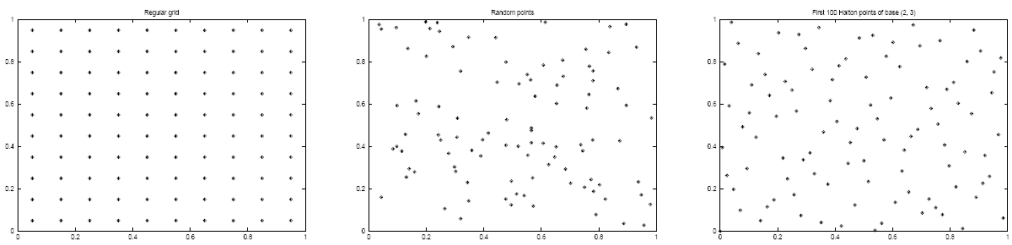

Figure 4.1: Left: 100 points distributed by a regular grid; Middle: 100 points distributed by a ordinary random number generator; Right: 100 points distributed by a quasi-random sequence (Halton low-discrepancy sequence). (image taken from [Las99])

In the next section we show a few sampling approaches which helps to minimize the noise from the images.

4.2.1 Importance Sampling

Importance sampling is variance reduction technique [And99]. Importance sampling is to chose a distribution $p(X)$ that is close to the integrand $f(X)$ which we want to estimate. The best estimator would ideally has zero variance. There are some properties which an importance sampling function $p(X)$ has to fulfil:

- $p(X) > 0$ if $f(x) \neq 0$ for the sample point x.

- it should be fast to sample from $p(X)$.
- $p(X)$ should be proportional to $f(X)$, like $p(X) * \alpha \geq f(X)$.
- it should be possible to compute the density $p(X)$ for any value of X.

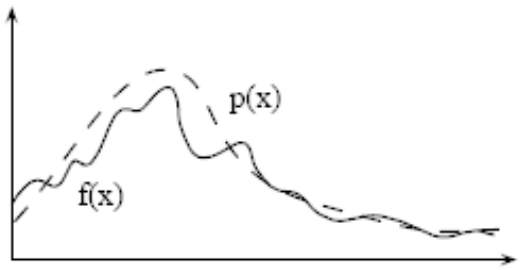

Figure 4.2: The continues function is the integrand f(x), which we want to estimate, and the dotted function the estimator p(x). In the case above our estimator p(x) has a low variance. (image taken form [Ghe07])

4.2.2 Inversion Sampling

The inversion method is only useable when the density function $p(X)$ is one dimensional and discrete (defined over a finite range). If the previous mentioned criterions met, then we have to compute the CDF $P(X)$ from the PDF $p(X)$ after that we calculate the inverse of the CDF $P(X)^{-1}$ then it is possible to generate random numbers that have the density p from a set of uniform distributed numbers ξ_i where $\xi_i \in [0,1]$.
There is a good example in [PH03] which clarify the usage of the inversion method. They use a discrete process with 4 possible outcomes, the PDF possible outcomes sum to 1. To create the CDF $P(X)$ we stack the bars on the top of each other, starting left. The rightmost bar must be one because all possibilities must sum to one. Now we can generate a uniform random number and project it to the CDF. The probability to hit a certain bar is the height of the bar.
There is an extended version of the inversion method in [PH04] which makes it possible to break down a high dimensional density function, so that we can use this sampling method.

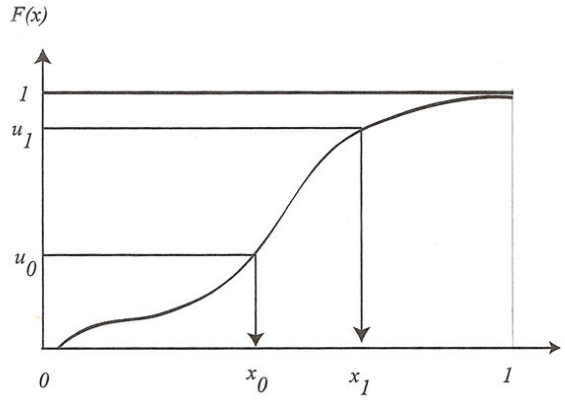

Figure 4.3: $x_1..x_i$ are samples with a distribution $p(x)$, by applying the inverse CDF of $p(x)$ to u - a uniform distributed random variable - we generate the samples with $x_i = F^{-1}(u_i)$. (image taken from [DBB03])

4.2.3 Rejection Sampling

The rejection method is used when the underlying density function has complex form (if it is a high dimensional function) which make it impossible to use the inversion method.
Rejection sampling is a specialization of importance sampling. When we want to sample a x_i according to a density function $p(X)$, the method works like this: we have to find a function $g(X)$ where a $p(X)$ is subset from $g(X)$ for all x_i over the domain; now we take a random sample from $p(X)$ and calculate the ratio between $p(X)/Mg(X)$ where M knows how to sample $g(X)$. Then we generate a uniform random variable $h \in [0,1]$; if $h < p(X)/Mg(X)$ then we accept the sample otherwise we reject it.
Rejection sampling depends on how tight $g(X)$ is chosen. Also, this methods become really slow if we have to sample high frequency BRDF data.

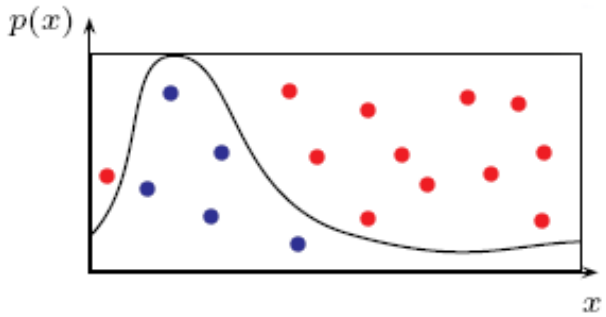

Figure 4.4: Rejection sampling: blue samples are accepted ($\in p(X)$), red samples are rejected ($\ni p(X)$). (image taken form [Ghe07])

Chapter 5

Implementation

In this chapter we present the implementation of this diploma thesis but also give a short introduction about the rendering toolkit which was used for the implementation.

5.1 Rendering in ART

Since 1996 the Institute of Computer Graphics and Algorithms of the Vienna University of Technology is developing a photorealistic rendering toolkit called ART (Advanced Rendering Toolkit). ART is a collection of several libraries which are separated according of their functionality. The libraries are written in a mix of ANSI C99 and Objective C, ANSI C99 is used for performance-critical modules and Objective-C for the high level modules. Modeling in ART is done through CSG, NURBS and subdivision surfaces, there is also a Turing-complete shading language available.
ART is a physical-based renderer, so there is a distinction between color, light and reflectance values to handle features like fluorescence or polarization are available, and several internal color types (at this time it is a compile option), ART is capable of using spectra instead of ordinary color values. The supported color types are Spectra with 8, 16 or 45 samples and also RGB and CIE XYZ color space, the latter two are mostly for reference purpose. The colorimetric accuracy is direct proportional to the number of samples, but with an increase of the sample number also the computation increase. There are also several publications out there which already used ART for their research e.g. Weidlich et al. [WW07], Wilkie et al. [WWLP06].
During the implementation we used ART as an ordinary RGB color space renderer with the MERL data and the Cornell RGB data but we also used ART as a Spectra renderer with Cornell Spectra data.

5.2 Data Representation

In this section we outline how we represent the measured BRDF data in memory and how we interpolate and sample the data. Hence we deal with different BRDF databases (MERL, Cornell) we have two different representation approaches.

5.2.1 Merl

The Merl data is saved in huge double arrays, but the ordering has sense. The sampling rate of the data is 90x90x180 ($\theta_h, \theta_d, \phi_d$), also the data is compressed with [Rus04]. So for each indicant and outgoing ray pair we have to transform to the Rusinkiewicz coordinate frame, the detailed calculation is described in appendix B.
The main issue with the data was that there was no explicit information about the color space in which the data lie, because the RGB data is mentioned in [Mat03] as:

$$f_r(\omega_i, \omega_o) = f_{sum}(\theta_h, \theta_d, \phi_d)$$

where f_r is the BRDF and f_{sum} is the sum of the three color channels for an indicant and outgoing ray. In Chapter 3 we already explained the acquisition process of data and know that the values that stored in the data set are no ordinary color values. The values are on one hand HDR values and on the other hand the sum of them are the BRDF value for the indicant and outgoing ray.
Also there was no need for any interpolation of the data sets due the dense measurements (90x90x180 = 1458000).

5.2.2 Cornell

The Cornell data representation is a bit more complicated, because there are four different file formats available, but all four formats follow the ASTM E1392-96 ASCII format (which is nothing than an ordinary text file with a descriptive header). The available formats are: RGB with negative red value (no gamut is applied); tristimulus values in CIE XYZ space; spectra with 31 wavelengths per indicant and outgoing ray-pair and 10nm sample distance; spectra with 65 wavelengths per indicant and outgoing ray-pair and 5nm sample distance. To index the color value spherical coordinates are used. One problem which occurred during the implementation was that the ϕ_o angle in every data set consists complete of negative values, except 0 and π. The data sets assume that they reciprocity hold, therefore only the data of the half sphere is available. Furthermore the Cornell data needs interpolation because the data is only measured every 10 degrees and it is only measured until 80 degrees.

The first approach for a memory presentation of the Cornell data was a KD-Tree, the nearest neighbor search is done in O(logN) [HMS06]. For the KD-Tree construction the variables θ_i, θ_o and ϕ_o are used to create the decisions nodes. The KD-Tree was a good data structure to index the BRDF data, but is a bad data structure for a trilinear interpolation because with the KD-Tree it is only possible to make linear interpolation.
The second approach for the data structure are something like a B*-Tree. The tree generation is constructed as following:

- Find all unique θ_i angles in the ASTM file (in a normal Cornell data set its about 10-11 data record) this angles build the first layer of root nodes.
- For each θ_i search all possible θ_o angles in the ASTM file and add this list of all possible θ_o as a seconde layer to the current node.
- Now we hold θ_i and θ_o and search for all possible ϕ_o and add them to the current θ_o node.
- Finally we sort the arrays ascending.

Figure 5.1 illustrate the Cornell data structure. The arrays are sorted with Quicksort and so we achieve the nearest neighbor search in each array in O(logN).

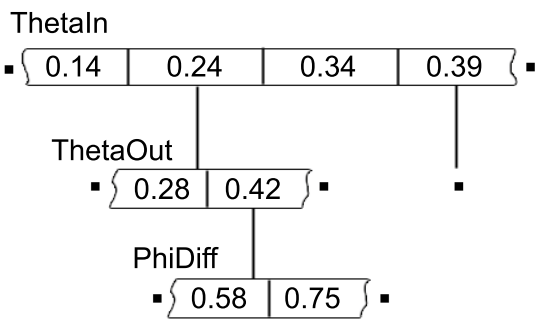

Figure 5.1: Cornell data representation

We introduced this structure for a fast trilinear interpolation approach. To present the approach we assume that we have the incoming and outgoing ray and already have transformed them to spherical coordinates. ϕ_{diff} is the difference angle between ϕ_i and ϕ_o, the difference angle is sufficient for the isotropic case. An important side note for the correct calculation of the ϕ_{diff} angle is that we first have to branch which ϕ (ϕ_i or ϕ_o) angle is greater then we subtract the smaller

one from the greater one; after this calculation we have also check if the ϕ_{diff} is greater then 2π; if so, we subtract ϕ_{diff} from 2π because due the reciprocity we only need a ϕ_{diff} in the range $[0,\pi]$.
For the trilinear interpolation we have, to compute several values which are needed:

- Begin with θ_i and search the nearest neighbor in the first layer (shown in Figure 5.1) then we check if the nearest neighbor is greater or smaller then the current θ_i. If it's greater, we create a new variable θ_{iUp} and as result of the prior sorting of the arrays we know that one index below in the array a θ-value is contained which is smaller than our θ_i. This is the θ_{iLow} variable.

- The above procedure is now done with θ_o, but for θ_{iUp} and θ_{iLow} for the index of the layer one. As a result we get four new variables: θ_{oUpUp}, θ_{oUpLow}, θ_{oLowUp}, $\theta_{oLowLow}$.

- Finally we compute the values for ϕ_{diff} but with the index values from layer one and two now we get eight values: $\phi_{diffUpUpUp}$, $\phi_{diffUpUpLow}$, $\phi_{diffUpLowUp}$, $\phi_{diffUpLowLow}$, $\phi_{diffLowUpUp}$, $\phi_{diffLowUpLow}$, $\phi_{diffLowLowUp}$, $\phi_{diffLowLowLow}$.

Figure 5.2 illustrate the acquisition of the variables for the interpolation. The interpolation variables are now used to index the color values (RGB or spectra data as described before) and use linear interpolation:

$$dst_i = aCol_i * (1-\lambda) + bCol_i * \lambda$$

where $aCol_i, bCol_i$ are the color channel values and dst_i is the computet color for the color channel i. λ is defined as:

$$\lambda = \frac{(a-x)^2}{(a-b)^2}$$

where x is the current point which lies between a and b. Thats one of the drawbacks of the interpolation - due to the fact that there is no data above 80 degrees (some data sets have no data above 75 degrees), x does not lie in between and then we cannot interpolate and fall back to nearest neighbor for the color lookup.

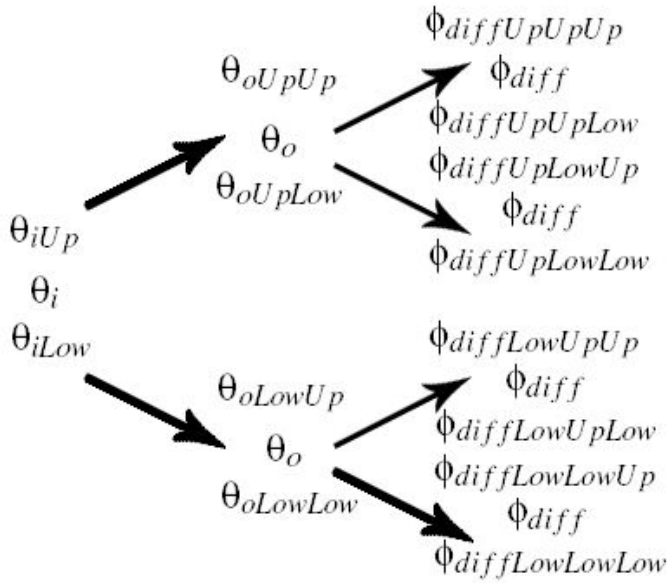

Figure 5.2: Trilinear interpolation

5.3 Rejection Sampling

In chapter 4 we already described what rejection sampling is in a general manner, in this section we present the way it is implemented for this thesis.
First the BRDF volume is separated into slices. Each slice has a fix θ_i and a θ_o and ϕ_diff is varying, θ_i is used to index the volume. Then we calculate the area of the cell and the maximum for each slice and save the resulting array to the hard disk to speed up the start up time for the next rendering process.
The maximum is defined as the sum of each channel. Note that the sum of the channels in the MERL data set is the BRDF value at this point. At the end we have to resample the complete BRDF with a regular grid. The grid cells have to be really small-so that we do not miss any BRDF value. The resampling of the Cornell data take about 15 minutes where the MERL data take more than 30 minutes.
Wtether to accept a ray or not is figured out through the decision equation:

$$ratio = \frac{f_{sum}(\theta_h, \theta_d, \phi_d)}{M_{slice}}$$

if the ratio is greater or equal than h (where h is a random variable between 0 and 1) then the ray is accepted otherwise it is rejected. To get the correct M_{slice} we use θ_i to index the correct volume, and here is the drawback of the approach. If the grid cells are not small enough it could happen that we miss a maximum value

and the rejection sample would not converge right.
The PDF is computed as:

$$pdf = \frac{f_{sum}(\theta_h, \theta_d, \phi_d)}{pdf_{slicePatch}} * \frac{1}{pdf_{curCel}}$$

where $pdf_{slicePatch}$ is precomputed during the resampling as:

$$pdf_{slicePatch} = \frac{2 * \pi * cos(\theta_o - samplingWidth) - cos(\theta_o)}{sampleCount}$$

and pdf_{curCel} is the cell area on the sphere surface. The pdf calculation worked with the Cornell data but gives some false results with the MERL data. After many trials to find a correct pdf we found that we got no errors if we use $f_{sum}(\theta_h, \theta_d, \phi_d)$ as pdf.

Chapter 6

Results

In this chapter we present our results in form of rendered images. Also polar plots were made for several angles. The polar plots were generated with a self made tool. The polar plots for each materials are illustrated in the appendix C.

6.1 MERL Renderings

The images were rendered with the ART pathtracer with lightsource sampling and 512 samples per pixel, an image resolution of 640x480 and with a recursion depth of five, all renderings made in RGB color space. We used a simple scene to test the renderings. As sampling technique rejection sampling is used, where the materials which are ideal diffuse or directional diffuse reflectors have a faster convergence than materials which are ideal specular or rough specular reflectors. Materials which are more diffuse were rendered approximately between 3 - 4 hours where the specular materials took between 12 - 15 hours. The most problematic material was Brass because the material has a tiny specular lobe, the rejection sampling with this material consumed the most time, because most of the sample points are rejected during the sample process.
For the polar plots three different angle combinations are used: $\theta_i = 45$ and $\theta_o = 45$; $\theta_i = 75$ and $\theta_o = 75$; $\theta_i = 85$ and $\theta_o = 85$.

6.1.1 Gold Metallic

Gold metallic paint has a metallic shine, with fine aluminum powder and pigments to get the metallic shine. This material has tiny bright spots caused by mirror like flakes. These spots are visible on grazing angles. The reflectance property is rough specular (glossy), as the polar plots show. Ngan et al. [NDM05] show that there is no analytical reflectance model that can reproduce the material with an

error under ~ 0.02, which they demonstrated in there experimental results which is in fact rather good, but not very surprising since the Cook-Torrance model was developed to simulate this material type.

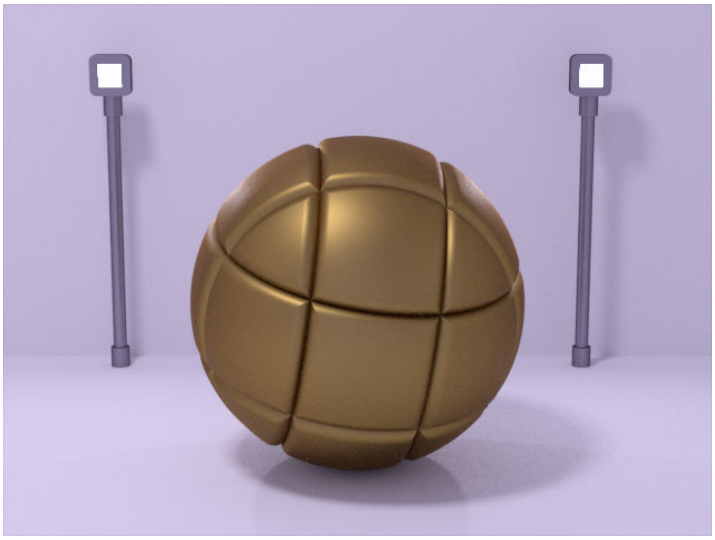

Figure 6.1: Gold Metallic

6.1.2 Aluminum Oxide

Aluminum oxide is also a paint with pigments,which has a better hiding (opacity) performance. The opacity is improved by optimal sizing the oxide particles. Aluminum oxide has sharp specular reflections. The reflectance property is directional diffuse, as the polar plots show. The experimental results of Ngan et al. [NDM05] show that the tested analytical reflectance models have almost the same reproduction performance with an error rate of ~ 0.08. The analytical models perform not as good as in the case of gold metallic paint since the normal Fresnel equations do not hold in the case of aluminum oxide.

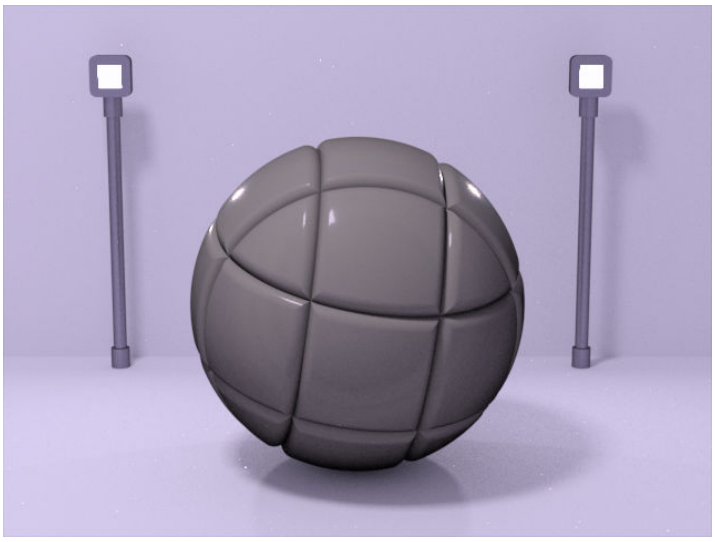

Figure 6.2: Aluminum Oxide

6.1.3 Blue Fabric

Blue fabric is a textile material, so they have a complex microfacet structure. It is nearly perfect diffuse except for grazing angles it produces rough specular reflection. This material has the fastest convergence of all rendered MERL materials in this thesis. As the polar plots show the material is ideal diffuse at the specular angle. The Lafortune et al. [LFTG97] reflectance model is able to reproduce the material with a small error of 0.000831 [NDM05].

Figure 6.3: Blue Fabric

6.1.4 Blue Rubber

Blue rubber is a rough surface which has specular highlights at grazing angles, where the highlights at the specular angle are soft which is difficult to see, the polar plots show sharp lobes at grazing angles but with a big diffuse component. The He et al. [HTSG91] model has the smallest reproduction error of 0.00134 [NDM05].

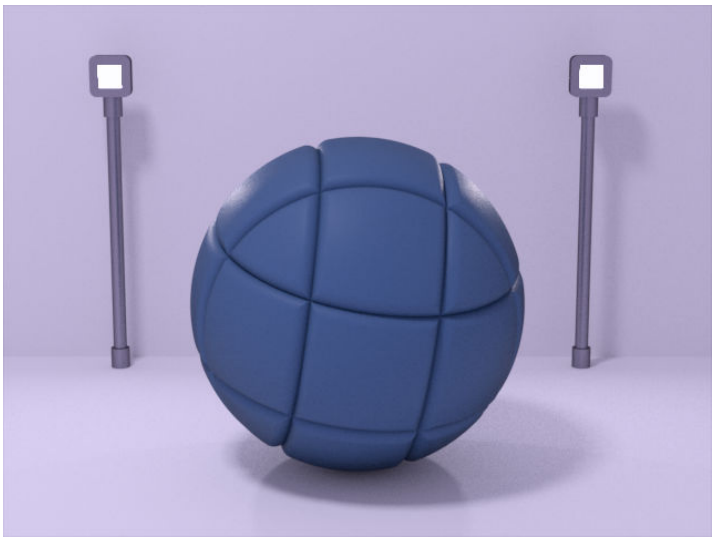

Figure 6.4: Blue Rubber

6.1.5 Pink Plastic

Pink plastic has specular highlights at grazing angles. Highlights at the specular angle are not visible on the rendering but it is visible on the polar plot as sharp lobe, the reason is that diffuse component is almost ideal so we accept more samples on the diffuse component of this material. The He et al. [HTSG91] model has the smallest reproduction error of 0.00406 [NDM05], but the reference image is more coarse grained than the simulation.

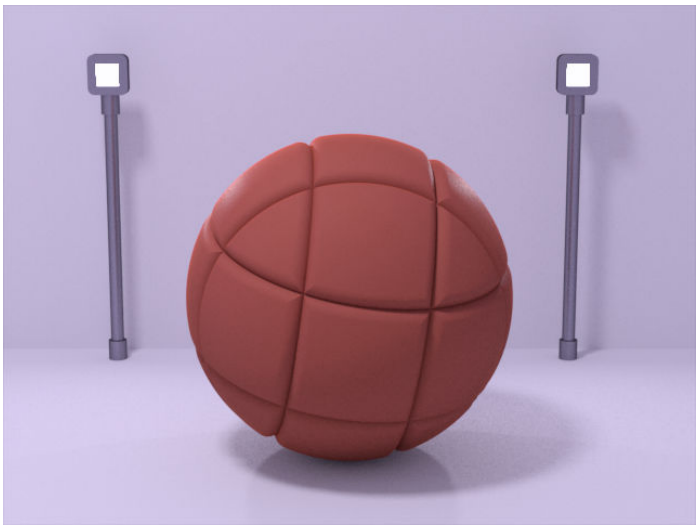

Figure 6.5: Pink Plastic

6.1.6 Purple Paint

Purple paint has also a rough surface with sharp specular highlights at grazing angles and it has also highlights at the specular angle(which are not as sharp as the highlights which occur at grazing angles). In the polar plots sharp specular lobes are visible. The He et al. [HTSG91] reflectance model outperform all analytically in [NDM05] with a error rate of 0.00613.

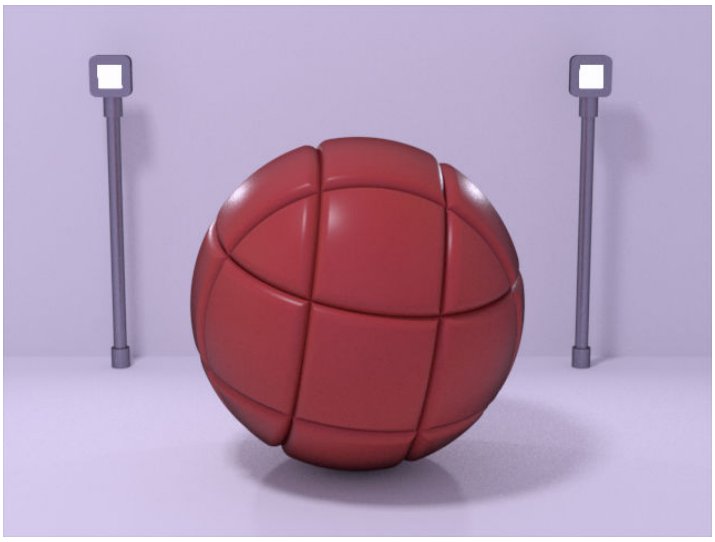

Figure 6.6: Purple Paint

6.1.7 Brass

Brass is an alloy of copper and zinc, copper has a cubic crystal system and the zinc atoms attach to the copper atoms without changing the crystal structure. The material has almost a ideal specular surface, as seen in the polar plots. It takes about 15 hours to simulate the material due the small lobe, the rejection sampling reject many sampling points. Also there are some errors in the date at grazing angles due the limits of the gonioreflectometer from Matusik [Mat03]. The analytical reflectance models in Ngan et al. [NDM05] have almost the same error rate of ~ 0.4.

Figure 6.7: Brass

6.2 Cornell Renderings

The Cornell data is rendered with 1024 samples and a recursion depth of five, all renderings made with the ART Spectra 8 renderer.
For the polar plots four different angle combinations are used: $\theta_i = 0$ and $\theta_o = 0$; $\theta_i = 15$ and $\theta_o = 15$; $\theta_i = 45$ and $\theta_o = 45$; $\theta_i = 75$ and $\theta_o = 75$. Only two samples are included in the thesis because the other material samples provided form the Cornell University are uncomplete, not interpolated and contain errors.

6.2.1 Garnet Red

Garnet Red is a spray paint with a low gloss component. The material is rendered twice; once it is rendered without interpolation and the second time with interpolation to show the interpolation effect. The materials have bright specular highlights at grazing angles and at the specular angle (see the polar plots). For certain angle the materials are almost ideal diffuse.

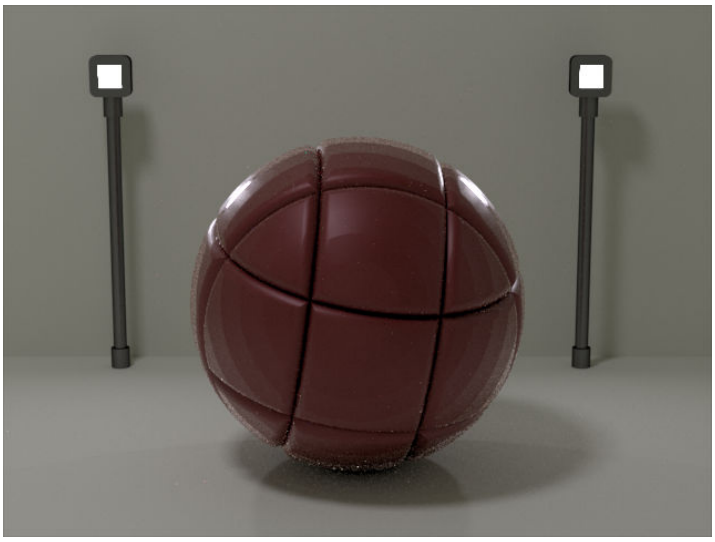

Figure 6.8: Garnet Red without interpolation and 256 samples. The rendering took thirty minutes.

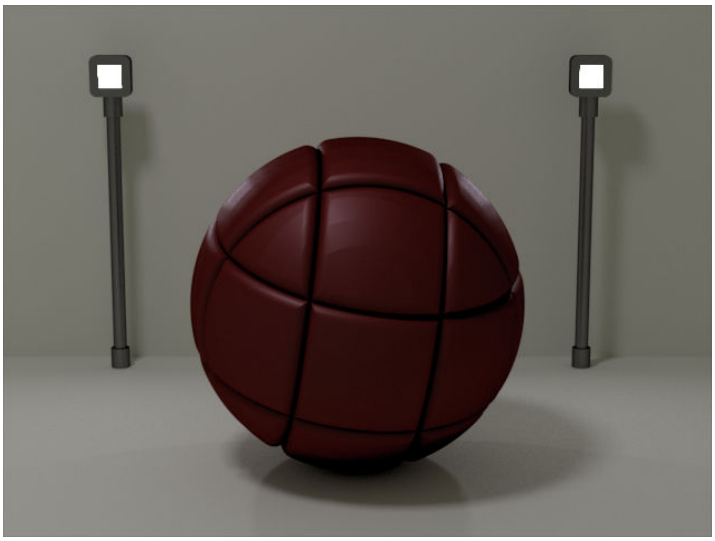

Figure 6.9: Garnet Red with interpolation and 1024 samples. The rendering took three hours.

6.2.2 Krylon Blue

Krylon Blue is also a spray paint with a low gloss component. It has the same reflectance characteristics as Garnet Red.

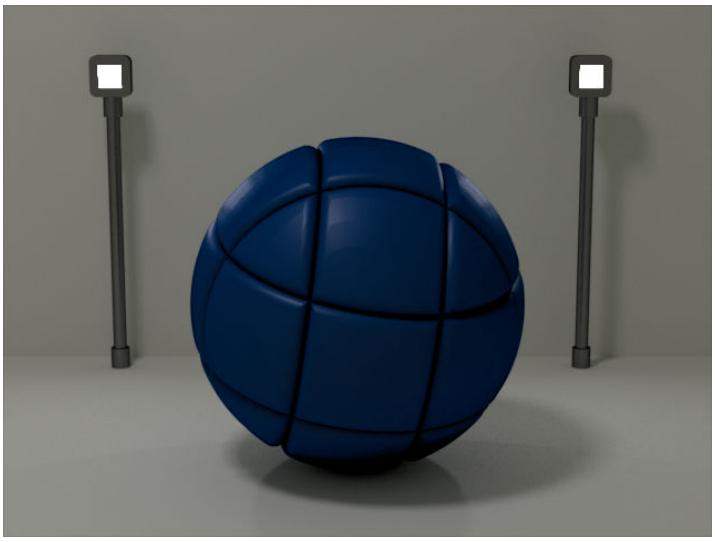

Figure 6.10: Krylon Blue with interpolation and 1024 samples.

Chapter 7

Conclusion

In this thesis we used two BRDF measurement databases for image synthesis with a photorealistic rendering toolkit, namely the Advanced Rendering Toolkit (ART), developed at the University of Technology Vienna. One of the challenges during the implementation was that there is almost no information on how to calculate a PDF for measured data. In this paper we tried to give the reader an overview about the important things which are needed to reproduce the images we generated using ART, but we tried also to go in depth were other paper and thesis do not. We presented a PDF formula for the Cornell database and also a data structure for trilinear interpolation. We also showed important details of the data set, which are not mentioned anywhere else. We rendered only a representative subset of the MERL data, because the fact that a rendering took between 3 - 15 hours. Due the design of ART it is also possible to use a measured BRDF surface n times with just one memory presentation of the data.
Also only isotropic measurements were used for the image synthesis but the data structure is already ready for anisotropic data. As we already mentioned in Chapter 3, MERL extended their library with some anisotropic materials.
The work is limited to make use of the measured data for direct rendering but with the MERL database it is possible to generate new BRDF's through linear combination. There are several new approaches to generate new BRDF's like BRDFShop ([MC06]).

Appendix A

Spherical Coordinates

Spherical coordinates are a natural way to describe a point which lies on a sphere. However, spherical coordinates are also used to index a BRDF value on the unit sphere in BRDF measurement data.
To describe a point we need the three variables (which are illustrated in Figure A.1):

- r is the distance from the origin of the sphere (the sphere radius)
- ϕ is the azimuth angle ($\phi \in [0, \frac{\pi}{2}]$)
- θ is the zenith angle ($\theta \in [0, 2\pi]$)

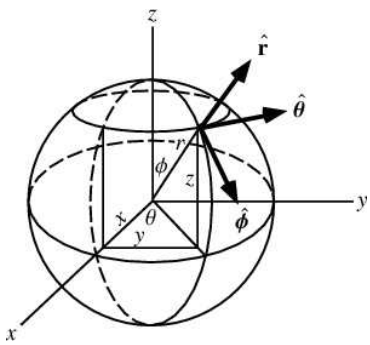

Figure A.1: Spherical coordinates: θ the azimuthal angle in the x, y plane; ϕ is the polar angle from the z-axis; r is the distance from the origin. (image taken from [Wei])

In ART we get the indicant and outgoing ray in cartesian coordinates, so first we have to convert these rays in spherical coordinates with r = 1 (unit sphere).

To convert a vector with x, y, z from cartesian coordinates to spherical coordinates:

$$r = \sqrt{x^2 + y^2 + z^2} \tag{1}$$

$$\theta = tan^{-1}\frac{y}{x} \tag{2}$$

$$\phi = cos^{-1}\frac{z}{r} \tag{3}$$

And to convert back to cartesian coordinates:

$$x = rcos\theta sin\phi \tag{4}$$

$$y = rsin\theta sin\phi \tag{5}$$

$$z = rcos\phi \tag{6}$$

Appendix B

Rusinkiewicz Coordinate Frame

Rusinkiewicz [Rus04] proposed a new coordinate frame which has several advantages as the ordinary BRDF coordinate frame (tangent-binormal-normal). Instead of $\theta_i, \phi_i, \theta_o, \phi_o$ the Rusinkiewicz coordinate frame proposed a parametrization along the halfway vector h (illustrated in Figure B.1) and a difference vector.

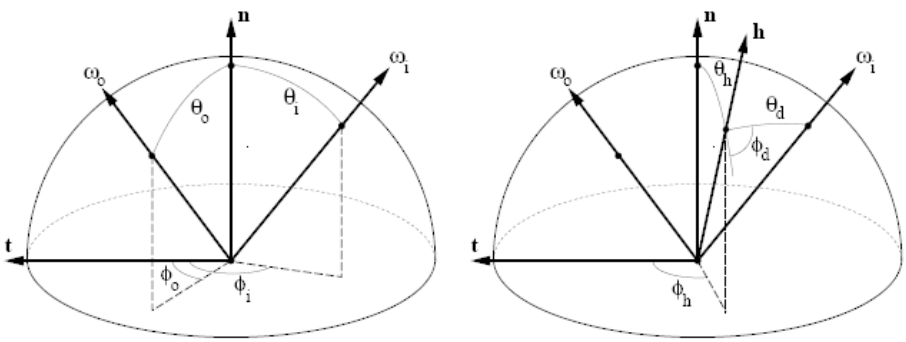

Figure B.1: Left: ordinary coordinate frame, Right: Rusinkiewicz coordinate frame. (image taken from [Rus04])

The transformation has several properties which are relevant: it needs less storage on isotropic BRDF data because ϕ_h is irrelevant; we save also storage due the fact that "*the BRDF has a strong dependence with each axis, but show only weak dependence on combonations of axes*" [Rus04]; the Helmholtz reciprocity depends only on $\phi_d \in \phi_d + \pi$.
Matusik [MPBM03] used the Rusinkiewicz presentation in their BRDF mea-

surements so that we needed to transform from the vector representation in the Rusinkiewiz coordinate frame. To do this we calculate the halfway vector h as:

$$h = \frac{\omega_i + \omega_o}{2} \tag{1}$$

where ω_i and ω_o are the incoming and outgoing ray (these two vectors are already in local space). Then we have to transform the halfway vector into spherical coordinates (with r = 1) and get θ_h and ϕ_h. To get θ_d and ϕ_d we need a difference vector which is calculated in two steps: first we rotate ω_i around the local normal vector with $-\phi_h$ as angle; after the first step we get a new vector which we rotate around the local binormal with $-\theta_h$ as angle; now we have the difference vector after the conversion in spherical coordinates we have the two angles θ_d and ϕ_d. To index the BRDF data from [MPBM03] we use θ_d, θ_h and ϕ_d.

Appendix C

BRDF Polar Plots

C.1 Gold Metallic

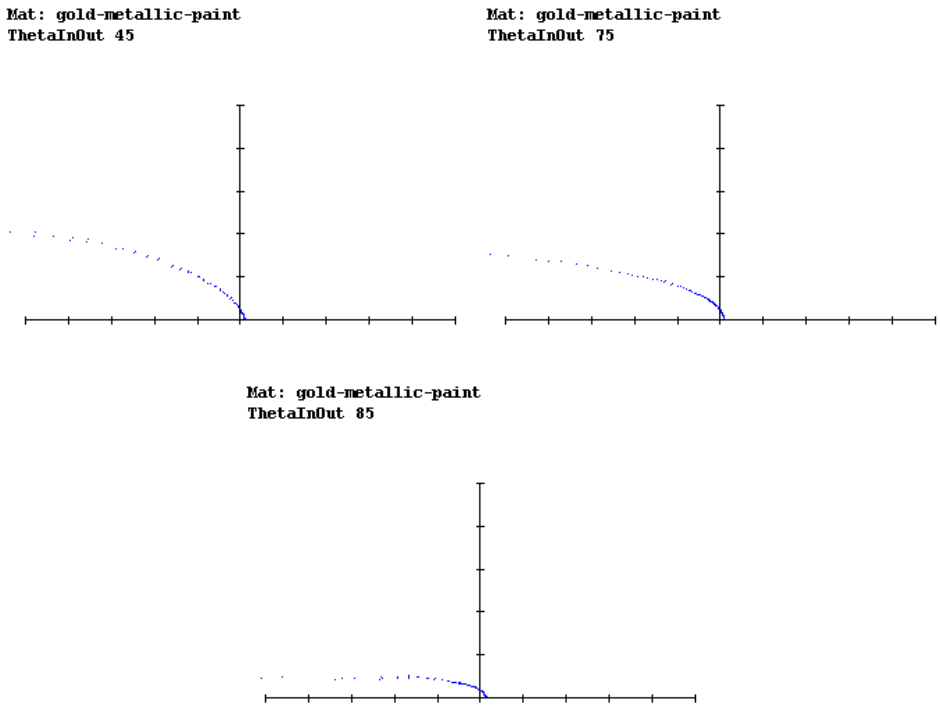

Figure C.1: Gold Metallic polar plots

C.2 Aluminum Oxide

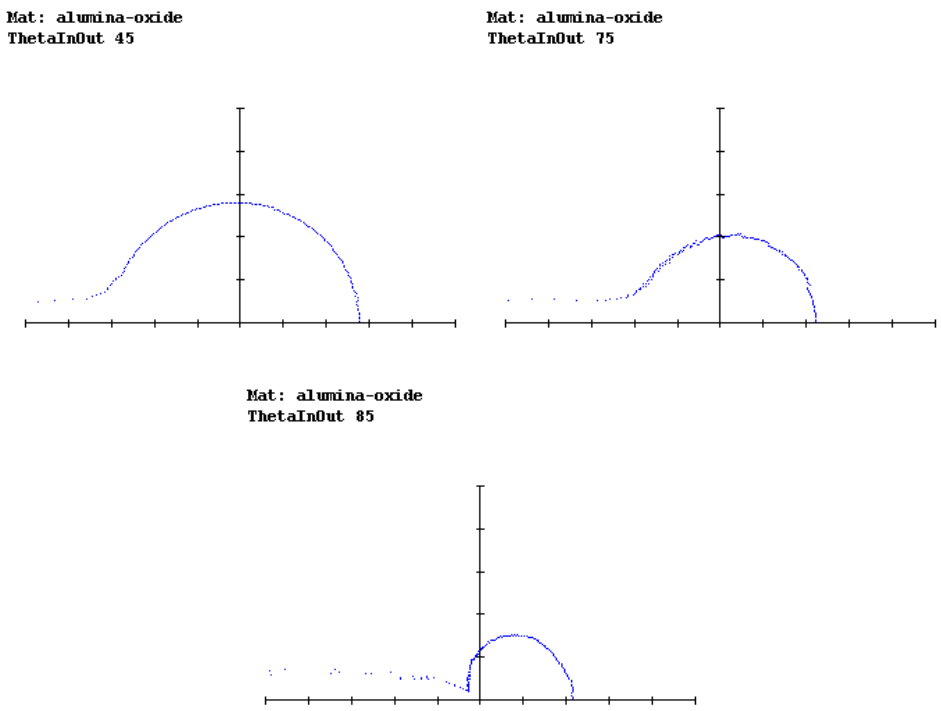

Figure C.2: Aluminum Oxide polar plots

C.3 Blue Fabric

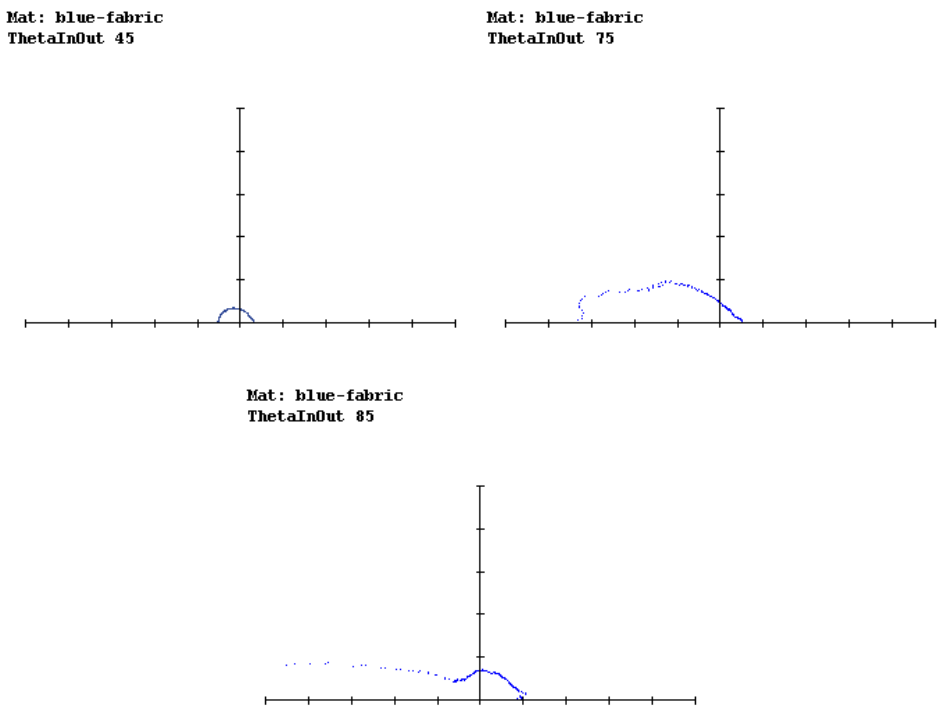

Figure C.3: Blue Fabric polar plots

C.4 Blue Rubber

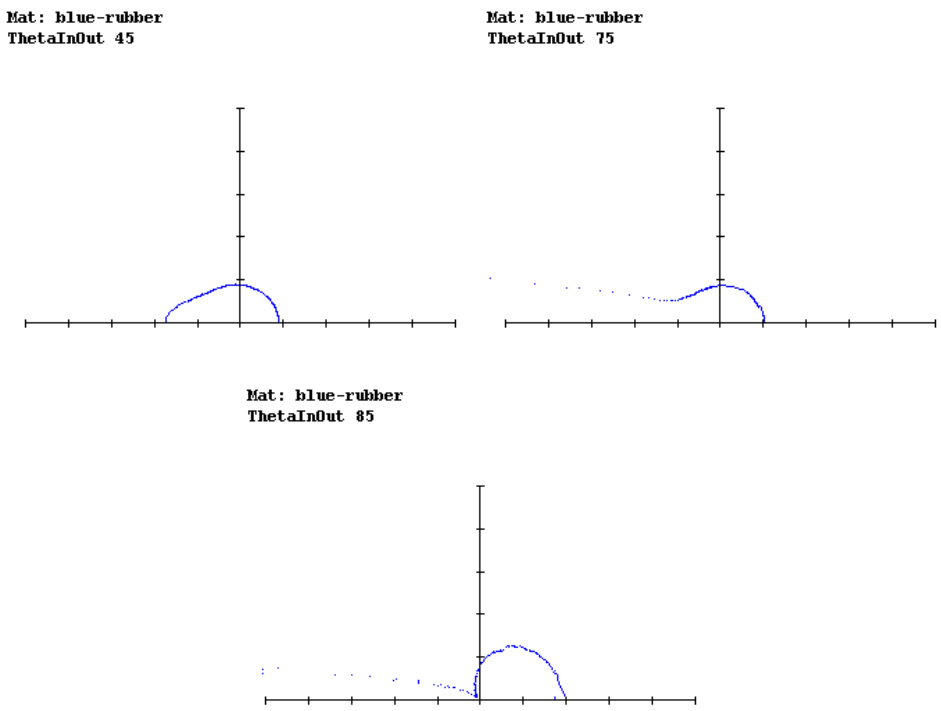

Figure C.4: Blue Rubber polar plots

C.5 Pink Plastic

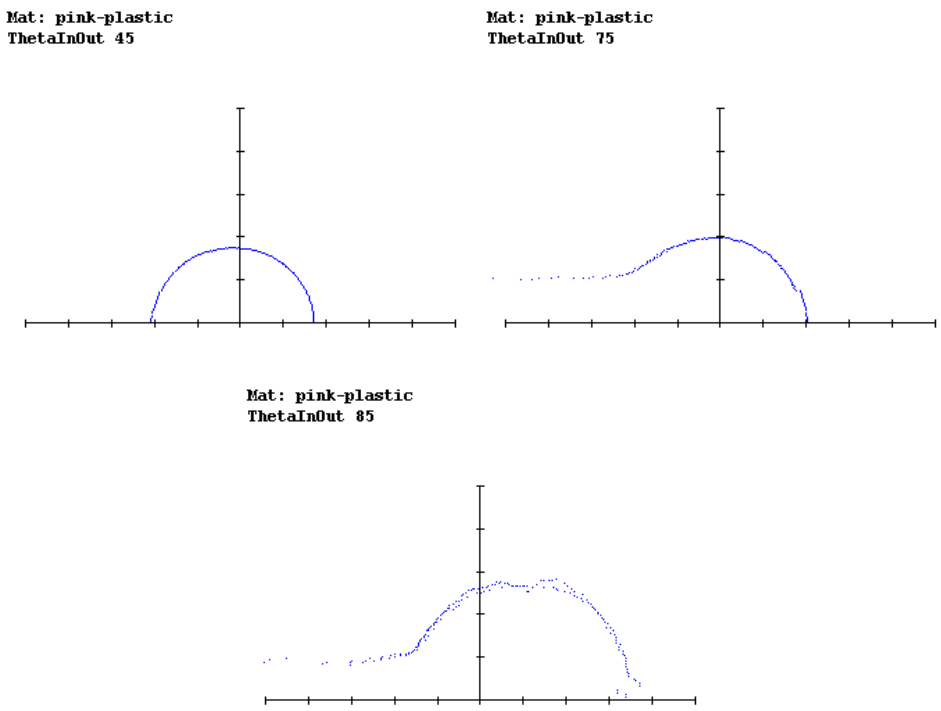

Figure C.5: Pink Plastic polar plots

C.6 Purple Paint

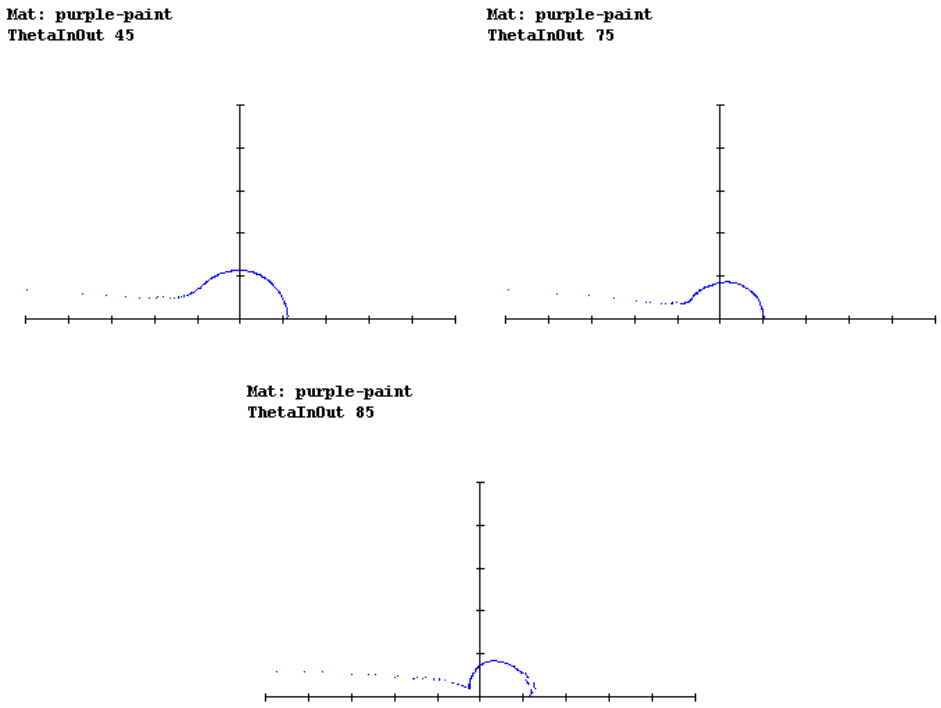

Figure C.6: Purple Paint polar plots

C.7 Brass

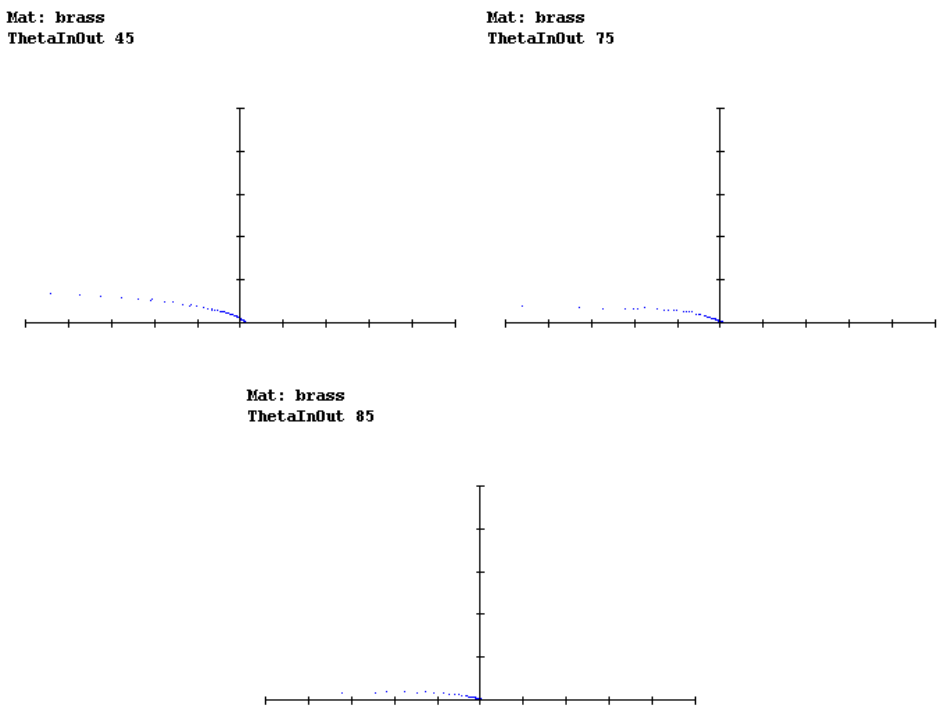

Figure C.7: Brass polar plots

C.8 Garnet Red

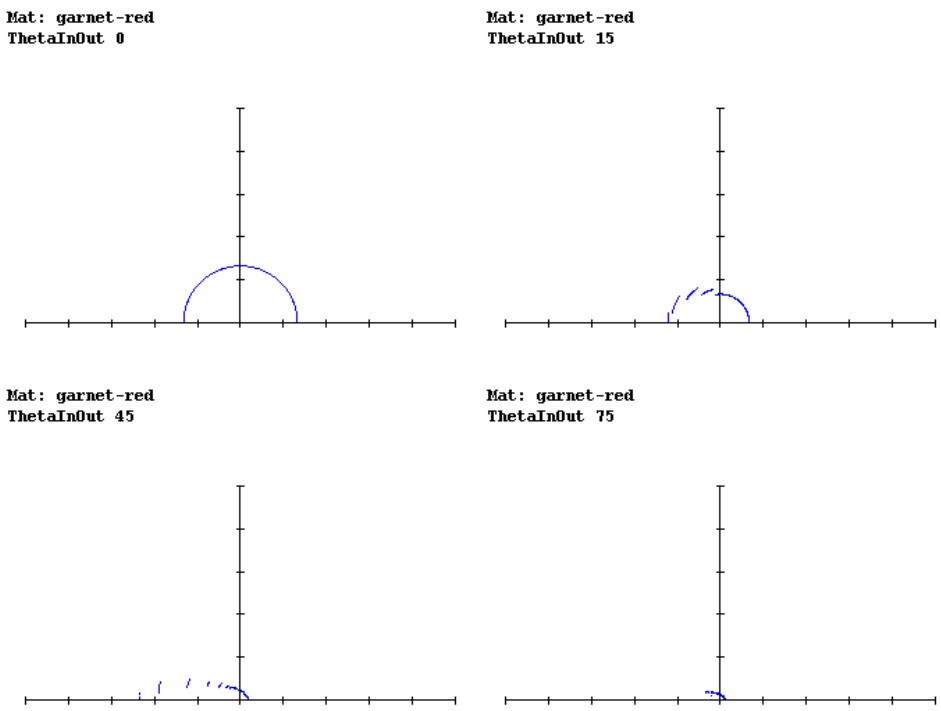

Figure C.8: Garnet Red polar plots

C.9 Krylon Blue

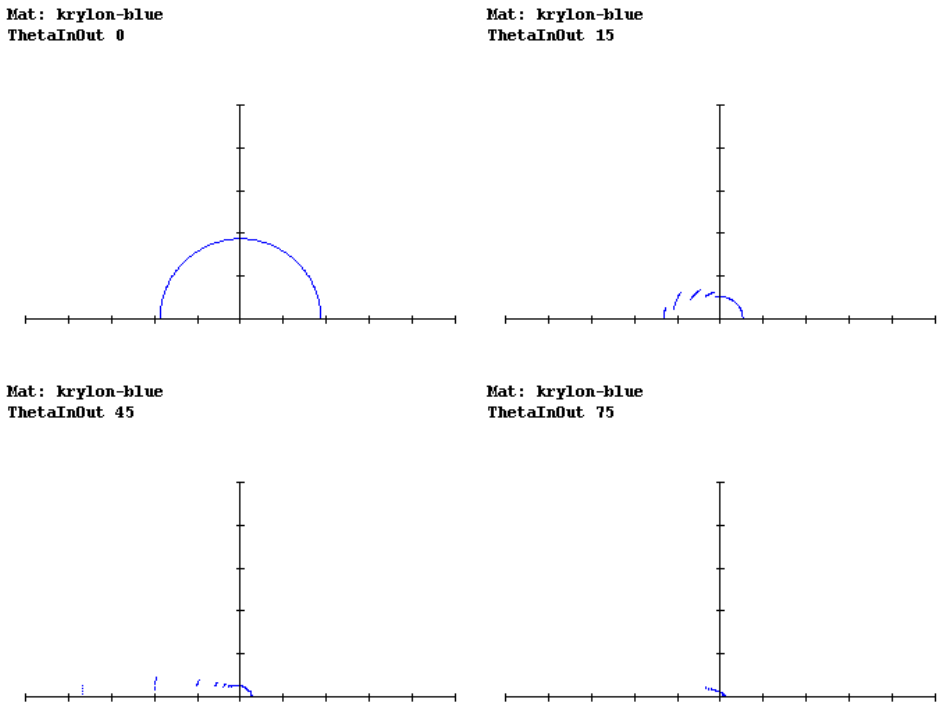

Figure C.9: Krylon Blue polar plots

List of Figures

Bibliography

[And99] Eric C. Anderson. Monte carlo methods and importance sampling. oct 1999.

[Bli77] James F. Blinn. Models of light reflection for computer synthesized pictures. *ACM*, pages 192–198, 1977.

[Bor03] George Borshukov. Measured brdf in film production - realistic cloth appearance for ”the matrix reloaded”. *ESC Entertainment*, 2003.

[Coo86] Robert L. Cook. Stochastic sampling in computer graphics. *ACM Trans. Graph.*, 5(1):51–72, 1986.

[CT82] R. L. Cook and K. E. Torrance. A reflectance model for computer graphics. *ACM Trans. Graph.*, 1(1):7–24, 1982.

[DBB03] Philip Dutre, Philippe Bekaert, and Kavita Bala. Advanced global illumination. 2003.

[DvGNK99] Kristin J. Dana, Bram van Ginneken, Shree K. Nayar, and Jan J. Koenderink. Reflectance and texture of real-world surfaces. *ACM Transactions on Graphics*, 18(1):1–34, 1999.

[Ein5a] Albert Einstein. On a heuristic viewpoint concerning the production and transformation of light. *Annalen der Physik 17*, pages 132–148, 1905a.

[Foo97] Sing Choong Foo. A gonioreflectometer for measuring the bidirectional reflectance of material for use in illumination computation. aug 1997.

[Geb03] Nikolaus Gebhardt. Einige brdf modelle. 2003.

[Ghe07] Mihai Calin Ghete. Mathematical basics of monte carlo rendering algorithms. 2007.

[HMS06] Warren Hunt, William R. Mark, and Gordon Stoll. Fast kd-tree construction with an adaptive error-bounded heuristic. *2006 IEEE Symposium on Interactive Ray Tracing*, Sept. 2006.

[HTSG91] Xiao D. He, Kenneth E. Torrance, François X. Sillion, and Donald P. Greenberg. A comprehensive physical model for light reflection. *ACM*, pages 175–186, 1991.

[Hua02] Jian Huang. Global illumination. *SIGGRAPH*, 2002.

[Huy78] Christiaan Huygens. Traite de la lumiere. 1678.

[Jen01] Henrik Wann Jensen. Monte carlo ray tracing for realistic image synthesis. State of the Art 39, Stanford University, aug 2001.

[JN86] Gerald H. Jacobs Jay Neitz. Polymorphism of the long-wavelength cone in normal human colour vision. *Nature 323*, pages 623 – 625, 1986.

[Kaj86] James T. Kajiya. The rendering equation. nov 1986.

[KET67] E. M. Sparrow K. E. Torrance. Theory for off-specular reflection from roughened surfaces. *Optical Society of America*, 57(9):1105–1114, sep 1967.

[KW86] M. Kalos and P. Whitlock. Monte carlo methods. *New York: Wiley and Sons*, 1986.

[Lam] Johann Heinrich Lambert. Lamberts cosine law. *Retrieved April 20, 2008, http://de.wikipedia.org/wiki/Lambertsches_Gesetz.*

[Las99] Szirmay-Kalos Laszlo. Monte-carlo methods in global illumination. 1999.

[Lew93] Robert R. Lewis. Making shaders more physically plausible. *Fourth Eurographics Workshop on Rendering*, (Series EG 93 RW):47–62, 1993.

[LFTG97] Eric P. F. Lafortune, Sing-Choong Foo, Kenneth E. Torrance, and Donald P. Greenberg. Non-linear approximation of reflectance functions. *ACM Press/Addison-Wesley Publishing Co*, pages 117–126, 1997.

[Mat03] Wojciech Matusik. *A Data-Driven Reflectance Model*. PhD thesis, Massachusetts Institute Of Technology, 2003.

[MC75] A.M. Smith Murray-Coleman, J.F. The automshd measurement of brdfs and their application to luminaire modeling. *Journal of the Illuminating Engineering Sociery*, 18(6):311–317, 1975.

[MC06] Jaroslav Krivanek Mark Colbert, Sumanta Pattanaik. Brdf-shop: Creating physically correct bidirectional reflectance distribution function. *IEEE Computer Society*, pages 30–36, jan 2006.

[MPBM03] Wojciech Matusik, Hanspeter Pfister, Matthew Brand, and Leonard McMillan. A data-driven reflectance model. *ACM Trans. Graph.*, 22(3):759–769, 2003.

[MWLT00] S. Marschner, S. Westin, E. Lafortune, and K. Torrance. Image-based brdf measurement. *S.R. Marschner, S.H. Westin, E.P.F. Lafortune, and K.E. Torrance. Image-Based BRDF measurement. Applied Optics, 39(16):2592–2600*, 2000.

[NDM05] Addy Ngan, Frdo Durand, and Wojciech Matusik. Experimental analysis of brdf models. *Eurographics Association*, pages 117–126, 2005.

[New04] Isaac Newton. Opticks or a treatise of the reflections, refractions, inflections and colours of light. 1704.

[ON95] M. Oren and S.K. Nayar. Generalization of the lambertian model and implications for machine vision. *IJCV*, 14(3):227–251, apr 1995.

[PH03] Matt Pharr and Greg Humphreys. *Physically-Based Image Synthesis From Theory To Implementation*. 4. nov 2003.

[PH04] Matt Pharr and Greg Humphreys. Infinite area light source with importance sampling. 2004.

[Pho75] Bui Tuong Phong. Illumination for computer generated pictures. *Commun. ACM*, 18(6):311–317, 1975.

[Rus04] Szymon M. Rusinkiewicz. A new change of variables for efficient brdf representation. *Proceedings of the 2004 SIGGRAPH Conference*, 23(3):496–505, aug 2004.

[SKN91] Takeo Kanade Shree K. Nayarm, Katsushi Ilkeuchi. Surface reflection: Physical and geometrical perspectives. *ACM*, 13:611–634, jul 1991.

[War92] Gregory J. Ward. Measuring and modeling anisotropic reflection. *ACM*, pages 265–272, jul 1992.

[Wei] Eric Weisstein. Spherical coordinates. *From MathWorld–A Wolfram Web Resource, http://mathworld.wolfram.com/SphericalCoordinates.html*.

[Wik] Wikipedia. Bidirectional scattering distribution function. *Retrieved April 20, 2008, http://en.wikipedia.org/wiki/Bidirectional_scattering_distribution_function*.

[Wil] Alexander Wilkie. Vorlesung einführung in die farbwissenschaft. *Lecture delivered 2005 at Technical University Vienna*.

[WW07] Andrea Weidlich and Alexander Wilkie. Arbitrarily layered microfacet surfaces. *GRAPHITE '07: Proceedings of the 5th international conference on Computer graphics and interactive techniques in Australia and Southeast Asia*, pages 171–178, 2007.

[WWLP06] Alexander Wilkie, Andrea Weidlich, Caroline Larboulette, and Werner Purgathofer. A reflectance model for diffuse fluorescent surfaces. *Proceedings of Graphite 2006*, pages 321–328, 2006.

[Wyn00] Chris Wynn. An introduction to brdf based lighting. Technical report, NVIDIA Corporation, 2000.

[You02] Thomas Young. The wave theory of light (pmm 259). 1802.